

Chapter 3

Chemical Speciation

3.1 Magnetism

3.1.1 Magnetics¹

3.1.1.1 Magnetic moments

The magnetic moment of a material is the incomplete cancellation of the atomic magnetic moments in that material. Electron spin and orbital motion both have magnetic moments associated with them (Figure 3.1), but in most atoms the electronic moments are oriented usually randomly so that overall in the material they cancel each other out (Figure 3.2), this is called diamagnetism.

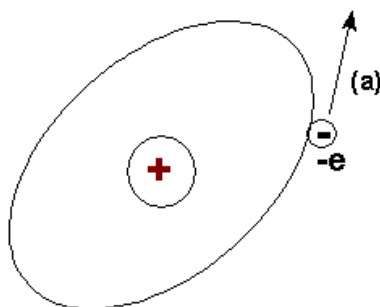


Figure 3.1: Orbital magnetic moment.

¹This content is available online at <<http://cnx.org/content/m22749/1.4/>>.

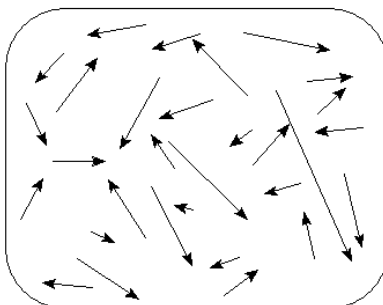


Figure 3.2: Magnetic moments in a diamagnetic sample.

If the cancellation of the moments is incomplete then the atom has a net magnetic moment. There are many subclasses of magnetic ordering such as para-, superpara-, ferro-, antiferro- or ferrimagnetism which can be displayed in a material and which usually depends, upon the strength and type of magnetic interactions and external parameters such as temperature and crystal structure atomic content and the magnetic environment which a material is placed in.

$$\mu_B = \frac{eh}{4\pi m} = 9.72 \times 10^{-24} \text{ J/T}$$

The magnetic moments of atoms, molecules or formula units are often quoted in terms of the Bohr magneton, which is equal to the magnetic moment due to electron spin

3.1.1.2 Magnetization

The magnetism of a material, the extent to which a material is magnetic, is not a static quantity, but varies compared to the environment that a material is placed in. It is similar to the temperature of a material. For example if a material is placed in an oven it will heat up to a temperature similar to that of the oven. However the speed of heating of that material, and also that of cooling are determined by the atomic structure of the material. The magnetization of a material is similar. When a material is placed in a magnetic field it may become magnetized to an extent and retain that magnetization after it is removed from the field. The extent of magnetization, and type of magnetization and the length of time that a material remains magnetized, depends again on the atomic makeup of the material.

Measuring a material's magnetism can be done on a micro or macro scale. Magnetism is measured over two parameters direction and strength. Thus magnetization has a vector quantity. The simplest form of a magnetometer is a compass. It measures the direction of a magnetic field. However more sophisticated instruments have been developed which give a greater insight into a material's magnetism.

So what exactly are you reading when you observe the output from a magnetometer?

The magnetism of a sample is called the magnetic moment of that sample and will be called that from now on. The single value of magnetic moment for the sample, is a combination of the magnetic moments on the atoms within the sample (Figure 3.3), it is also the type and level of magnetic ordering and the physical dimensions of the sample itself.

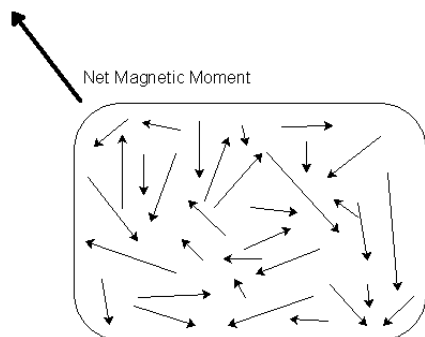


Figure 3.3: Schematic representations of the net magnetic moment in a diamagnetic sample.

The "intensity of magnetization", M , is a measure of the magnetization of a body. It is defined as the magnetic moment per unit volume or

$$M = m/V$$

with units of Am (emucm³ in cgs notation).

A material contains many atoms and their arrangement affects the magnetization of that material. In Figure 3.4 (a) a magnetic moment m is contained in unit volume. This has a magnetization of m Am. Figure 3.4 (b) shows two such units, with the moments aligned parallel. The vector sum of moments is $2m$ in this case, but as the both the moment and volume are doubled M remains the same. In Figure 3.4 (c) the moments are aligned antiparallel. The vector sum of moments is now 0 and hence the magnetization is 0 Am.

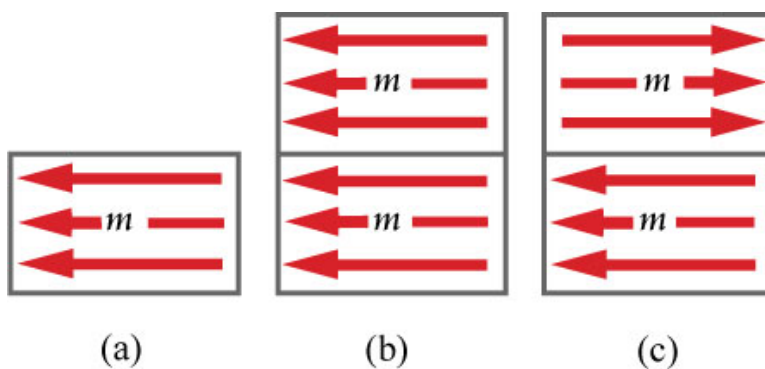


Figure 3.4: Effect of moment alignment on magnetization: (a) Single magnetic moment, (b) two identical moments aligned parallel and (c) antiparallel to each other. Adapted from J. Bland Thesis M. Phys (Hons)., 'A Mossbauer spectroscopy and magnetometry study of magnetic multilayers and oxides.' Oliver Lodge Labs, Dept. Physics, University of Liverpool

Scenarios (b) and (c) are a simple representation of ferro- and antiferromagnetic ordering. Hence we would expect a large magnetization in a ferromagnetic material such as pure iron and a small magnetization

in an antiferromagnet such as $\gamma\text{-Fe}_2\text{O}_3$

3.1.1.3 Magnetic Response

When a material is passed through a magnetic field it is affected in two ways:

1. Through its susceptibility.
2. Through its permeability.

3.1.1.3.1 Magnetic susceptibility

The concept of magnetic moment is the starting point when discussing the behavior of magnetic materials within a field. If you place a bar magnet in a field it will experience a torque or *moment* tending to align its axis in the direction of the field. A compass needle behaves in the same way. This torque increases with the strength of the poles and their distance apart. So the value of magnetic moment tells you, in effect, 'how big a magnet' you have.

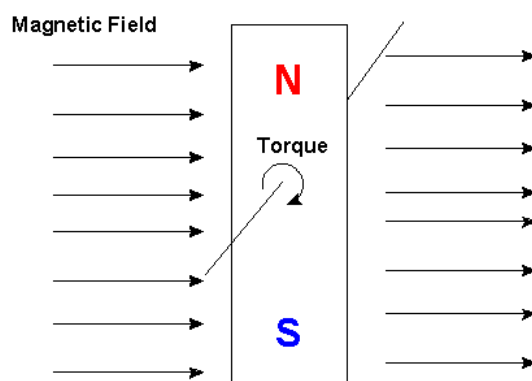


Figure 3.5: Schematic representation of the torque or moment that a magnet experiences when it is placed in a magnetic field. The magnet will try to align with the magnetic field.

If you place a material in a weak magnetic field, the magnetic field may not overcome the binding energies that keep the material in a non magnetic state. This is because it is energetically more favorable for the material to stay exactly the same. However, if the strength of the magnetic moment is increased, the torque acting on the smaller moments in the material, it may become energetically more preferable for the material to become magnetic. The reasons that the material becomes magnetic depends on factors such as crystal structure the temperature of the material and the strength of the field that it is in. However a simple explanation of this is that as the magnetic moment strength increases it becomes more favorable for the small fields to align themselves along the path of the magnetic field, instead of being opposed to the system. For this to occur the material must rearrange its magnetic makeup at the atomic level to lower the energy of the system and restore a balance.

It is important to remember that when we consider the magnetic susceptibility and take into account how a material changes on the atomic level when it is placed in a magnetic field with a certain moment. The moment that we are measuring with our magnetometer is the total moment of that sample.

$$\chi = \frac{M}{H}$$

where χ = susceptibility, M = variation of magnetization, and H = applied field.

3.1.1.3.2 Magnetic permeability

Magnetic permeability is the ability of a material to conduct an electric field. In the same way that materials conduct or resist electricity, materials also conduct or resist a magnetic flux or the flow of magnetic lines of force (Figure 3.6).

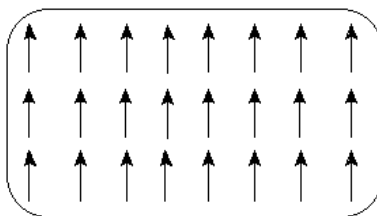


Figure 3.6: Magnetic ordering in a ferromagnetic material.

Ferromagnetic materials are usually highly permeable to magnetic fields. Just as electrical conductivity is defined as the ratio of the current density to the electric field strength, so the magnetic permeability, μ , of a particular material is defined as the ratio of flux density to magnetic field strength. However unlike in electrical conductivity magnetic permeability is nonlinear.

$$\mu = \mathbf{B}/\mathbf{H}$$

Permeability, where μ is written without a subscript, is known as absolute permeability. Instead a variant is used called relative permeability.

$$\mu = \mu_0 \times \mu_r$$

Absolute permeability is a variation upon 'straight' or absolute permeability, μ , but is more useful as it makes clearer how the presence of a particular material affects the relationship between flux density and field strength. The term 'relative' arises because this permeability is defined in relation to the permeability of a vacuum, μ_0 .

$$\mu_r = \mu/\mu_0$$

For example, if you use a material for which $\mu_r = 3$ then you know that the flux density will be three times as great as it would be if we just applied the same field strength to a vacuum.

3.1.1.3.2.1 Initial permeability

Initial permeability describes the relative permeability of a material at low values of B (below 0.1 T). The maximum value for μ in a material is frequently a factor of between 2 and 5 or more above its initial value.

Low flux has the advantage that every ferrite can be measured at that density without risk of saturation. This consistency means that comparison between different ferrites is easy. Also, if you measure the inductance with a normal component bridge then you are doing so with respect to the initial permeability.

3.1.1.3.2 Permeability of a vacuum in the SI

The permeability of a vacuum has a finite value - about $1.257 \times 10^{-6} \text{ H m}^{-1}$ - and is denoted by the symbol μ_0 . Note that this value is constant with field strength and temperature. Contrast this with the situation in ferromagnetic materials where μ is strongly dependent upon both. Also, for practical purposes, most non-ferromagnetic substances (such as wood, plastic, glass, bone, copper aluminum, air and water) have permeability almost equal to μ_0 ; that is, their relative permeability is 1.0.

The permeability, μ , the variation of magnetic induction,

$$B = \mu_0(H + M)$$

with applied field,

$$\mu = B/H$$

3.1.1.4 Background contributions

A single measurement of a sample's magnetization is relatively easy to obtain, especially with modern technology. Often it is simply a case of loading the sample into the magnetometer in the correct manner and performing a single measurement. This value is, however, the sum total of the sample, any substrate or backing and the sample mount. A sample substrate can produce a substantial contribution to the sample total.

For substrates that are diamagnetic, under zero applied field, this means it has no effect on the measurement of magnetization. Under applied fields its contribution is linear and temperature independent. The diamagnetic contribution can be calculated from knowledge of the volume and properties of the substrate and subtracted as a constant linear term to produce the signal from the sample alone. The diamagnetic background can also be seen clearly at high fields where the sample has reached saturation: the sample saturates but the linear background from the substrate continues to increase with field. The gradient of this background can be recorded and subtracted from the readings if the substrate properties are not known accurately.

3.1.1.5 Hysteresis

When a material exhibits hysteresis, it means that the material responds to a force and has a history of that force contained within it. Consider if you press on something until it depresses. When you release that pressure, if the material remains depressed and doesn't spring back then it is said to exhibit some type of hysteresis. It remembers a history of what happened to it, and may exhibit that history in some way. Consider a piece of iron that is brought into a magnetic field, it retains some magnetization, even after the external magnetic field is removed. Once magnetized, the iron will stay magnetized indefinitely. To demagnetize the iron, it is necessary to apply a magnetic field in the opposite direction. This is the basis of memory in a hard disk drive.

The response of a material to an applied field and its magnetic hysteresis is an essential tool of magnetometry. Paramagnetic and diamagnetic materials can easily be recognized, soft and hard ferromagnetic materials give different types of hysteresis curves and from these curves values such as saturation magnetization, remnant magnetization and coercivity are readily observed. More detailed curves can give indications of the type of magnetic interactions within the sample.

3.1.1.6 Diamagnetism and paramagnetism

The intensity of magnetization depends upon both the magnetic moments in the sample and the way that they are oriented with respect to each other, known as the magnetic ordering.

Diamagnetic materials, which have no atomic magnetic moments, have no magnetization in zero field. When a field is applied a small, negative moment is induced on the diamagnetic atoms proportional to the applied field strength. As the field is reduced the induced moment is reduced.

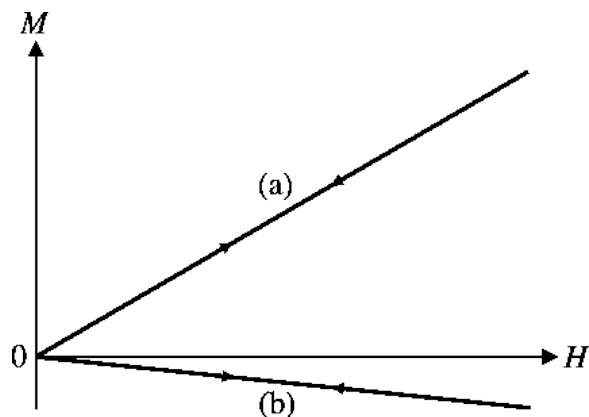


Figure 3.7: Typical effect on the magnetization, M , of an applied magnetic field, H , on (a) a paramagnetic system and (b) a diamagnetic system. Adapted from J. Bland Thesis M. Phys (Hons), 'A Mossbauer spectroscopy and magnetometry study of magnetic multilayers and oxides.' Oliver Lodge Labs, Dept. Physics, University of Liverpool

In a paramagnet the atoms have a net magnetic moment but are oriented randomly throughout the sample due to thermal agitation, giving zero magnetization. As a field is applied the moments tend towards alignment along the field, giving a net magnetization which increases with applied field as the moments become more ordered. As the field is reduced the moments become disordered again by their thermal agitation. The figure shows the linear response $M \propto H$ where $\mu H \ll kT$.

3.1.1.7 Ferromagnetism

The hysteresis curves for a ferromagnetic material are more complex than those for diamagnets or paramagnets. Below diagram shows the main features of such a curve for a simple ferromagnet.

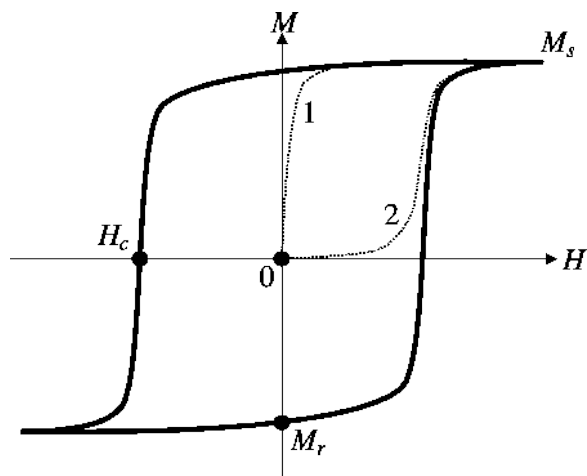


Figure 3.8: Schematic of a magnetization hysteresis loop in a ferromagnetic material showing the saturation magnetization, M_s , coercive field, H_c , and remnant magnetization, M_r . Virgin curves are shown dashed for nucleation (1) and pinning (2) type magnets. Adapted from J. Bland Thesis M. Phys (Hons), 'A Mossbauer spectroscopy and magnetometry study of magnetic multilayers and oxides.' Oliver Lodge Labs, Dept. Physics, University of Liverpool

In the virgin material (point 0) there is no magnetization. The process of magnetization, leading from point 0 to saturation at $M = M_s$, is outlined below. Although the material is ordered ferromagnetically it consists of a number of ordered domains arranged randomly giving no net magnetization. This is shown in below (a) with two domains whose individual saturation moments, M_s , lie antiparallel to each other.

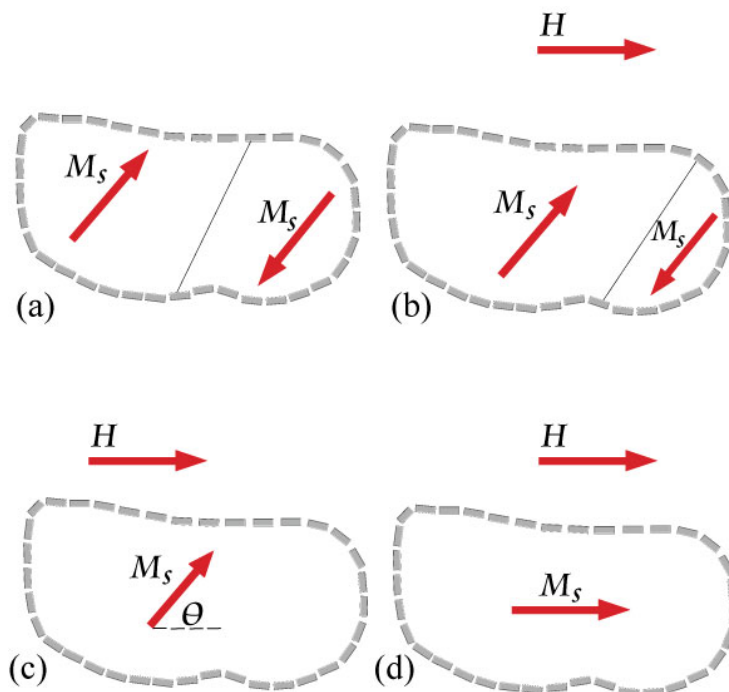


Figure 3.9: The process of magnetization in a demagnetized ferromagnet. Adaped from J. Bland Thesis M. Phys (Hons)., 'A Mossbauer spectroscopy and magnetometry study of magnetic multilayers and oxides.' Oliver Lodge Labs, Dept. Physics, University of Liverpool

As the magnetic field, H , is applied, (b), those domains which are more energetically favorable increase in size at the expense of those whose moment lies more antiparallel to H . There is now a net magnetization; M . Eventually a field is reached where all of the material is a single domain with a moment aligned parallel, or close to parallel, with H . The magnetization is now $M = M_s \cos \theta$ where θ is the angle between M_s along the easy magnetic axis and H . Finally M_s is rotated parallel to H and the ferromagnet is saturated with a magnetization $M = M_s$.

The process of domain wall motion affects the shape of the virgin curve. There are two qualitatively different modes of behavior known as nucleation and pinning, shown in Figure 3.8 as curves 1 and 2, respectively.

In a nucleation-type magnet saturation is reached quickly at a field much lower than the coercive field. This shows that the domain walls are easily moved and are not pinned significantly. Once the domain structure has been removed the formation of reversed domains becomes difficult, giving high coercivity. In a pinning-type magnet fields close to the coercive field are necessary to reach saturation magnetization. Here the domain walls are substantially pinned and this mechanism also gives high coercivity.

3.1.1.8 Remnance

As the applied field is reduced to 0 after the sample has reached saturation the sample can still possess a remnant magnetization, M_r . The magnitude of this remnant magnetization is a product of the saturation magnetization, the number and orientation of easy axes and the type of anisotropy symmetry. If the axis of anisotropy or magnetic easy axis is perfectly aligned with the field then $M_r = M_s$, and if perpendicular

$M_r = 0$.

At saturation the angular distribution of domain magnetizations is closely aligned to H . As the field is removed they turn to the nearest easy magnetic axis. In a cubic crystal with a positive anisotropy constant, K_1 , the easy directions are $\langle 100 \rangle$. At remnance the domain magnetizations will lie along one of the three $\langle 100 \rangle$ directions. The maximum deviation from H occurs when H is along the $\langle 111 \rangle$ axis, giving a cone of distribution of 55° around the axis. Averaging the saturation magnetization over this angle gives a remnant magnetization of $0.832 M_s$.

3.1.1.9 Coercivity

The coercive field, H_c , is the field at which the remnant magnetization is reduced to zero. This can vary from a few Am for soft magnets to 10^7 Am for hard magnets. It is the point of magnetization reversal in the sample, where the barrier between the two states of magnetization is reduced to zero by the applied field allowing the system to make a Barkhausen jump to a lower energy. It is a general indicator of the energy gradients in the sample which oppose large changes of magnetization.

The reversal of magnetization can come about as a rotation of the magnetization in a large volume or through the movement of domain walls under the pressure of the applied field. In general materials with few or no domains have a high coercivity whilst those with many domains have a low coercivity. However, domain wall pinning by physical defects such as vacancies, dislocations and grain boundaries can increase the coercivity.

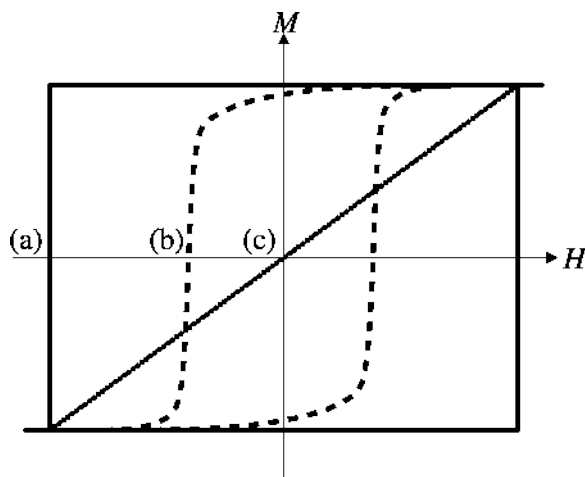


Figure 3.10: Shape of hysteresis loop as a function of Θ_H , the angle between anisotropy axis and applied field H , for: (a) $\Theta_H = 0^\circ$, (b) 45° and (c) 90° . Adapted from J. Bland Thesis M. Phys (Hons)., 'A Mossbauer spectroscopy and magnetometry study of magnetic multilayers and oxides.' Oliver Lodge Labs, Dept. Physics, University of Liverpool

The loop illustrated in Figure 3.10 is indicative of a simple bi-stable system. There are two energy minima: one with magnetization in the positive direction, and another in the negative direction. The depth of these minima is influenced by the material and its geometry and is a further parameter in the strength of the coercive field. Another is the angle, Θ_H , between the anisotropy axis and the applied field. The above fig shows how the shape of the hysteresis loop and the magnitude of H_c varies with Θ_H . This effect shows the importance of how samples with strong anisotropy are mounted in a magnetometer when comparing loops.

3.1.1.10 Temperature dependence

A hysteresis curve gives information about a magnetic system by varying the applied field but important information can also be gleaned by varying the temperature. As well as indicating transition temperatures, all of the main groups of magnetic ordering have characteristic temperature/magnetization curves. These are summarized in Figure 3.11 and Figure 3.12. At all temperatures a diamagnet displays only any magnetization induced by the applied field and a small, negative susceptibility.

The curve shown for a paramagnet (Figure 3.11) is for one obeying the Curie law,

$$\chi = \frac{C}{T}$$

and so intercepts the axis at $T = 0$. This is a subset of the Curie-Weiss law,

$$\chi = \frac{C}{T - \theta}$$

where θ is a specific temperature for a particular substance (equal to 0 for paramagnets).

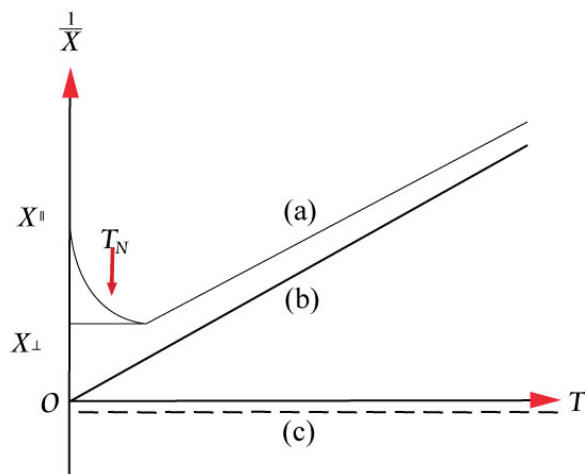


Figure 3.11: Variation of reciprocal susceptibility with temperature for: (a) antiferromagnetic, (b) paramagnetic and (c) diamagnetic ordering. Adapted from J. Bland Thesis M. Phys (Hons)., 'A Mossbauer spectroscopy and magnetometry study of magnetic multilayers and oxides.' Oliver Lodge Labs, Dept. Physics, University of Liverpool

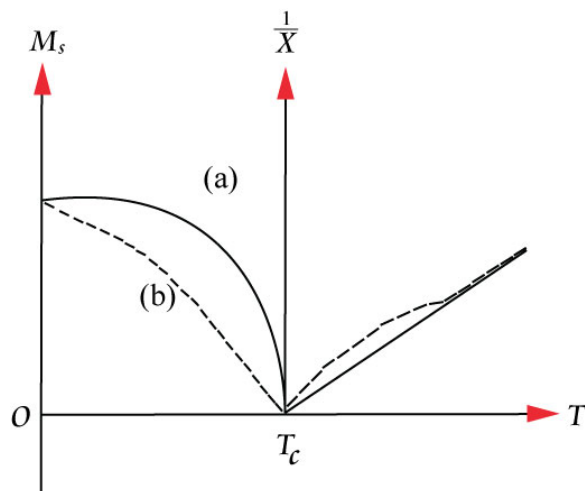


Figure 3.12: Variation of saturation magnetization below, and reciprocal susceptibility above T_c for: (a) ferromagnetic and (b) ferrimagnetic ordering. Adapted from J. Bland Thesis M. Phys (Hons.), 'A Mossbauer spectroscopy and magnetometry study of magnetic multilayers and oxides.' Oliver Lodge Labs, Dept. Physics, University of Liverpool

Above T_N and T_C both antiferromagnets and ferromagnets behave as paramagnets with $1/\chi$ linearly proportional to temperature. They can be distinguished by their intercept on the temperature axis, $T = \Theta$. Ferromagnetics have a large, positive Θ , indicative of their strong interactions. For paramagnetics $\Theta = 0$ and antiferromagnetics have a negative Θ .

The net magnetic moment per atom can be calculated from the gradient of the straight line graph of $1/\chi$ versus temperature for a paramagnetic ion, rearranging Curie's law to give

$$\mu = \sqrt{\frac{3Ak}{N_x}}$$

where A is the atomic mass, k is Boltzmann's constant, N is the number of atoms per unit volume and x is the gradient.

Ferromagnets below T_C display spontaneous magnetization. Their susceptibility above T_C in the paramagnetic region is given by the Curie-Weiss law

where g is the gyromagnetic constant. In the ferromagnetic phase with T greater than T_C the magnetization $M(T)$ can be simplified to a power law, for example the magnetization as a function of temperature can be given by

$$M(T) \approx (T_c - T)^\beta$$

where the term β is typically in the region of 0.33 for magnetic ordering in three dimensions.

The susceptibility of an antiferromagnet increases to a maximum at T_N as temperature is reduced, then decreases again below T_N . In the presence of crystal anisotropy in the system this change in susceptibility depends on the orientation of the spin axes: χ (parallel) decreases with temperature whilst χ (perpendicular) is constant. These can be expressed as

$$\chi \perp = \frac{C}{2\theta}$$

where C is the Curie constant and Θ is the total change in angle of the two sublattice magnetizations away from the spin axis, and

$$\chi_{\parallel} = \frac{2n_g \mu_H^2 B'(J, a'_0)}{2kT + n_g \mu_H^2 \gamma \rho B'(J, a'_0)}$$

where n_g is the number of magnetic atoms per gramme, B' is the derivative of the Brillouin function with respect to its argument a' , evaluated at a'_0 , μ_H is the magnetic moment per atom and γ is the molecular field coefficient.

3.1.1.11 Bibliography

- U. Gradmann, Handbook of Magnetic Materials, vol. 7.
- B. D. Cullity, *Introduction to Magnetic Materials*, Addison-Wesley, Massachusetts (1972).
- G. Bertotti, *Hysteresis in Magnetism*, Academic Press, San Diego (1998).
- S. Chikazumi, S. H. Charap, *Physics of Magnetism*, Krieger Publishing Company (1978).
- J. Bland, Thesis M. Phys (Hons)., 'A Mossbauer spectroscopy and magnetometry study of magnetic multilayers and oxides.' Oliver Lodge Labs, Dept. Physics, University of Liverpool.

3.1.2 Theory of A Superconducting Quantum Interference Device (SQUID)²

3.1.2.1 Introduction

One of the most sensitive forms of magnetometry is SQUID magnetometry. This technique uses a combination of superconducting materials and Josephson junctions to measure magnetic fields with resolutions up to $\sim 10^{-14}$ kG or greater. In the proceeding pages we will describe how a SQUID actually works.

3.1.2.2 Electron-pair waves

In superconductors the resistanceless current is carried by pairs of electrons, known as Cooper Pairs. A Cooper Pair is a pair of electrons. Each electron has a quantized wavelength. With a Cooper pair each electrons wave couples with its opposite number over a large distances. This phenomenon is a result of the very low temperatures at which many materials will superconduct.

What exactly is superconductance? When a material is at very low temperatures, its crystal lattice behaves differently than when it higher temperatures. Usually at higher temperatures a material will have large vibrations called in the crystal lattice. These vibrations scatter electrons as they pass through this lattice (Figure 3.13), and this is the basis for bad conductance.

²This content is available online at <<http://cnx.org/content/m22750/1.3/>>.

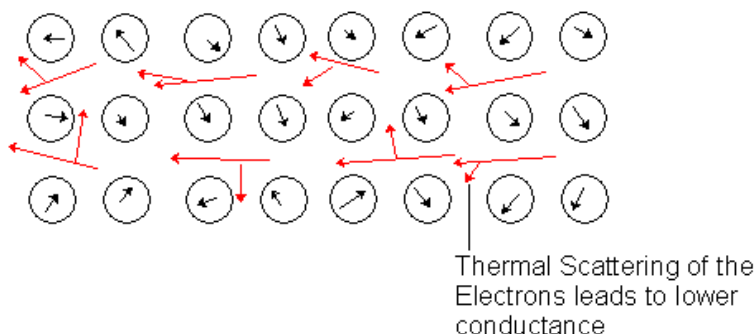


Figure 3.13: Schematic representation of the scattering of electrons as they pass through a vibrating lattice.

With a superconductor the material is designed to have very small vibrations, these vibrations are lessened even more by cooling the material to extremely low temperatures. With no vibrations there is no scattering of the electrons and this allows the material to superconduct.

The origin of a Cooper pair is that as the electron passes through a crystal lattice at superconducting temperatures its negative charge pulls on the positive charge of the nuclei in the lattice through coulombic interactions producing a ripple. An electron traveling in the opposite direction is attracted by this ripple. This is the origin of the coupling in a Cooper pair (Figure 3.14).

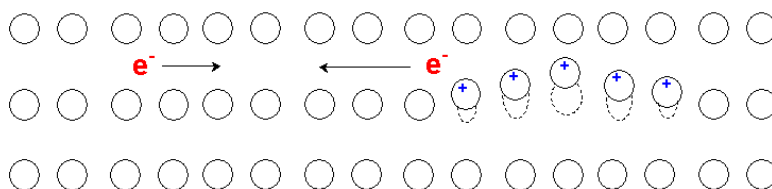


Figure 3.14: Schematic representation of the Cooper pair coupling model.

A passing electron attracts the lattice, causing a slight ripple toward its path. Another electron passing in the opposite direction is attracted to that displacement (Figure 3.15).

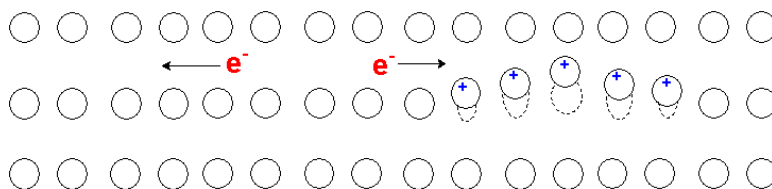


Figure 3.15: Schematic representation of Cooper pair coupling

Due to the coupling and the fact that for each pair there is two spin states (Figure 3.16).

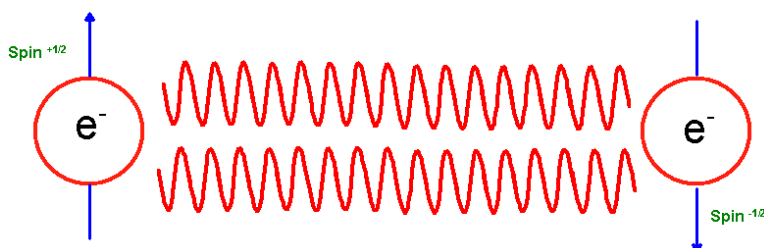


Figure 3.16: Schematic representation of the condensation of the wavelengths of a Cooper pairs

Each pair can be treated as a single particle with a whole spin, not half a spin such as is usually the case with electrons. This is important, as an electron which is classed in a group of matter called Fermions are governed by the Fermi exclusion principle which states that anything with a spin of one half cannot occupy the same space as something with the same spin of one half. This turns the electron means that a Cooper pair is in fact a Boson the opposite of a Fermion and this allows the Coopers pairs to condensate into one wave packet. Each Coopers pair has a mass and charge twice that of a single electron, whose velocity is that of the center of mass of the pair. This coupling can only happen in extremely cold conditions as thermal vibrations become greater than the force that an electron can exert on a lattice. And thus scattering occurs.

Each pair can be represented by a wavefunction of the form

$$\Phi_P = \Phi e^{i(P.r)/\hbar}$$

where P is the net momentum of the pair whose center of mass is at r . However, all the Cooper pairs in a superconductor can be described by a single wavefunction yet again due to the fact that the electrons are in a Coopers pair state and are thus Bosons in the absence of a current because all the pairs have the same phase - they are said to be "phase coherent"

$$\Psi_P = \Psi e^{i(P.r)/\hbar}$$

This electron-pair wave retains its phase coherence over long distances, and essentially produces a standing wave over the device circuit. In a SQUID there are two paths which form a circle and are made with the same standing wave (Figure 3.17). The wave is split in two sent off along different paths, and then recombined to record an interference pattern by adding the difference between the two.

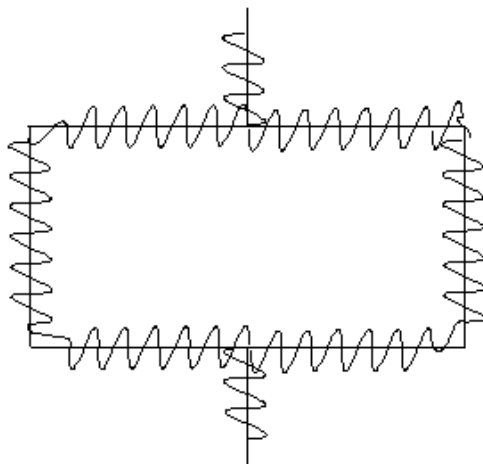


Figure 3.17: Schematic representation of a standing wave across a SQUID circuit.

This allows measurement at any phase differences between the two components, which if there is no interference will be exactly the same, but if there is a difference in their path lengths or in some interaction that the waves encounters such as a magnetic field it will correspond in a phase difference at the end of each path length.

A good example to use is of two water waves emanating from the same point. They will stay in phase if they travel the same distance, but will fall out of phase if one of them has to deviate around an obstruction such as a rock. Measuring the phase difference between the two waves then provides information about the obstruction.

3.1.2.3 Phase and coherence

Another implication of this long range coherence is the ability to calculate phase and amplitude at any point on the wave's path from the knowledge of its phase and amplitude at any single point, combined with its wavelength and frequency. The wavefunction of the electron-pair wave in the above eqn. can be rewritten in the form of a one-dimensional wave as

$$\Psi_p = \Psi \sin 2\pi \left(\frac{x}{\lambda} - vt \right)$$

If we take the wave frequency, V , as being related to the kinetic energy of the Cooper pair with a wavelength, λ , being related to the momentum of the pair by the relation $\lambda = h/p$ then it is possible to evaluate the phase difference between two points in a current carrying superconductor.

If a resistanceless current flows between points X and Y on a superconductor there will be a phase difference between these points that is constant in time.

3.1.2.4 Effect of a magnetic field

The parameters of a standing wave are dependent on a current passing through the circuit; they are also strongly affected by an applied magnetic field. In the presence of a magnetic field the momentum, p , of a particle with charge q in the presence of a magnetic field becomes $mV + qA$ where A is the magnetic vector potential. For electron-pairs in an applied field their moment P is now equal to $2mV + 2eA$.

In an applied magnetic field the phase difference between points X and Y is now a combination of that due to the supercurrent and that due to the applied field.

3.1.2.5 The fluxoid

One effect of the long range phase coherence is the quantization of magnetic flux in a superconducting ring. This can either be a ring, or a superconductor surrounding a non-superconducting region. Such an arrangement can be seen in Figure 3.18 where region N has a flux density B within it due to supercurrents flowing around it in the superconducting region S.

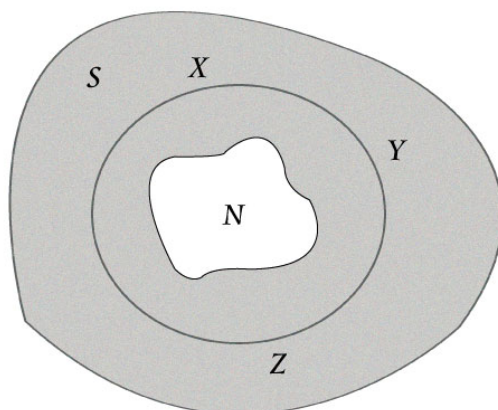


Figure 3.18: Superconductor enclosing a non-superconducting region. Adaped from J. Bland Thesis M. Phys (Hons)., 'A Mossbauer spectroscopy and magnetometry study of magnetic multilayers and oxides.' Oliver Lodge Labs, Dept. Physics, University of Liverpool.

In the closed path XYZ encircling the non-superconducting region there will be a phase difference of the electron-pair wave between any two points, such as X and Y, on the curve due to the field and the circulating current.

If the superelectrons are represented by a single wave then at any point on XYZX it can only have one value of phase and amplitude. Due to the long range coherence the phase is single valued also called quantized meaning around the circumference of the ring $\Delta\phi$ must equal $2\pi n$ where n is any integer. Due to the wave only having a single value the fluxoid can only exist in quantized units. This quantum is termed the fluxon, ϕ_0 , given by

$$\Phi_0 = \frac{h}{2e} = 2.07 \times 10^{-15} \text{ Wb}$$

3.1.2.6 Josephson tunneling

If two superconducting regions are kept totally isolated from each other the phases of the electron-pairs in the two regions will be unrelated. If the two regions are brought together then as they come close electron-pairs will be able to tunnel across the gap and the two electron-pair waves will become coupled. As the separation

decreases, the strength of the coupling increases. The tunneling of the electron-pairs across the gap carries with it a superconducting current as predicted by B.D. Josephson and is called "Josephson tunneling" with the junction between the two superconductors called a "Josephson junction" (Figure 3.19).

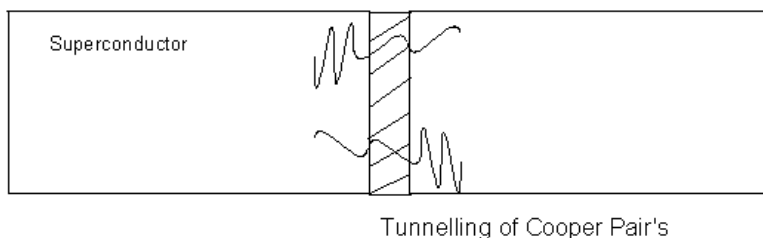


Figure 3.19: Schematic representation of the tunneling of Cooper pairs across a Josephson junction.

The Josephson tunneling junction is a special case of a more general type of weak link between two superconductors. Other forms include constrictions and point contacts but the general form is of a region between two superconductors which has a much lower critical current and through which a magnetic field can penetrate.

3.1.2.7 Superconducting quantum interference device (SQUID)

A superconducting quantum interference device (SQUID) uses the properties of electron-pair wave coherence and Josephson Junctions to detect very small magnetic fields. The central element of a SQUID is a ring of superconducting material with one or more weak links called Josephesons Junctions. An example is shown in the below. With weak-links at points W and X whose critical current, i_c , is much less than the critical current of the main ring. This produces a very low current density making the momentum of the electron-pairs small. The wavelength of the electron-pairs is thus very long leading to little difference in phase between any parts of the ring.

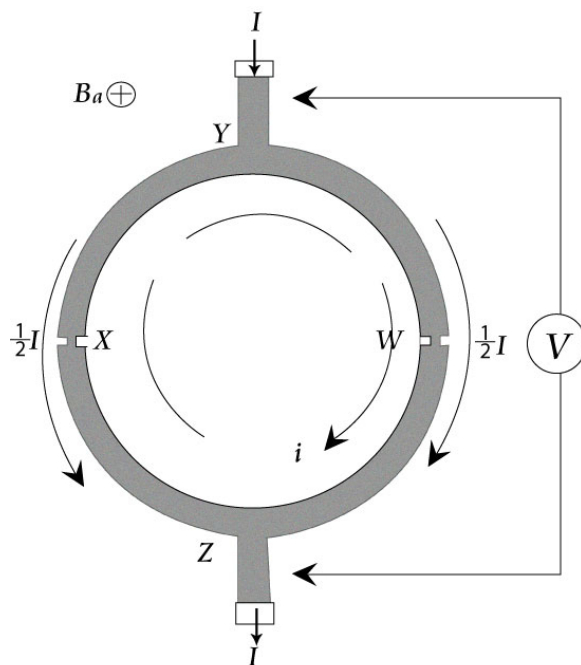


Figure 3.20: Superconducting quantum interference device (SQUID) as a simple magnetometer. Adapted from J. Bland Thesis M. Phys (Hons)., 'A Mossbauer spectroscopy and magnetometry study of magnetic multilayers and oxides.' Oliver Lodge Labs, Dept. Physics, University of Liverpool.

If a magnetic field, B_a , is applied perpendicular to the plane of the ring (Figure 3.21), a phase difference is produced in the electron-pair wave along the path XYW and WZX . One of the features of a superconducting loop is that the magnetic flux, Φ , passing through it which is the product of the magnetic field and the area of the loop and is quantized in units of $\Phi_0 = h / (2e)$, where h is Planck's constant, $2e$ is the charge of the Cooper pair of electrons, and Φ_0 has a value of 2×10^{-15} tesla m^2 . If there are no obstacles in the loop, then the superconducting current will compensate for the presence of an arbitrary magnetic field so that the total flux through the loop (due to the external field plus the field generated by the current) is a multiple of Φ_0 .

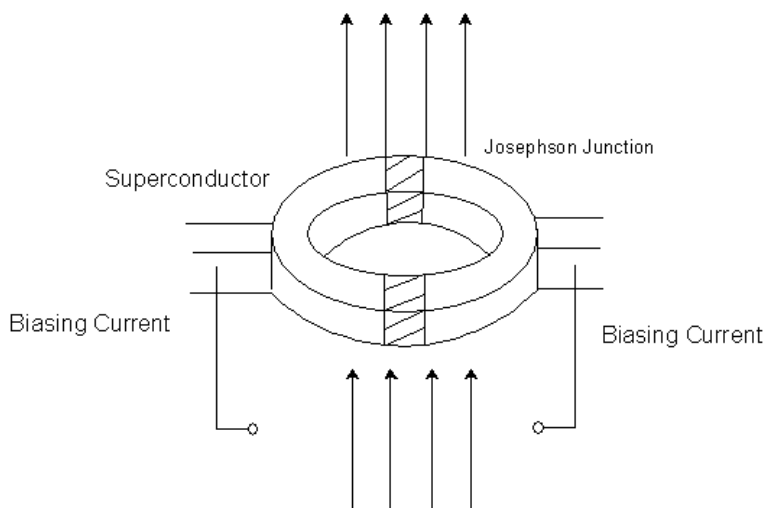


Figure 3.21: Schematic representation of a SQUID placed in a magnetic field.

Josephson predicted that a superconducting current can be sustained in the loop, even if its path is interrupted by an insulating barrier or a normal metal. The SQUID has two such barriers or ‘Josephson junctions’. Both junctions introduce the same phase difference when the magnetic flux through the loop is 0 , Φ_0 , $2\Phi_0$ and so on, which results in constructive interference, and they introduce opposite phase difference when the flux is $\Phi_0/2$, $3\Phi_0/2$ and so on, which leads to destructive interference. This interference causes the critical current density, which is the maximum current that the device can carry without dissipation, to vary. The critical current is so sensitive to the magnetic flux through the superconducting loop that even tiny magnetic moments can be measured. The critical current is usually obtained by measuring the voltage drop across the junction as a function of the total current through the device. Commercial SQUIDS transform the modulation in the critical current to a voltage modulation, which is much easier to measure.

An applied magnetic field produces a phase change around a ring, which in this case is equal

$$\Delta\phi(B) = 2\pi \frac{\Phi_a}{\Phi_0}$$

where Φ_a is the flux produced in the ring by the applied magnetic field. The magnitude of the critical measuring current is dependent upon the critical current of the weak-links and the limit of the phase change around the ring being an integral multiple of 2π . For the whole ring to be superconducting the following condition must be met

$$\alpha + \beta + 2\pi \frac{\Phi_a}{\Phi_0} = n \cdot 2\pi$$

where α and β are the phase changes produced by currents across the weak-links and $2\pi\Phi_a/\Phi_0$ is the phase change due to the applied magnetic field.

When the measuring current is applied α and β are no longer equal, although their sum must remain constant. The phase changes can be written as

$$\alpha = \pi \left[n - \frac{\Phi_a}{\Phi_o} \right] - \delta$$

$$\beta = \pi \left[n - \frac{\Phi_a}{\Phi_o} \right] + \delta$$

where δ is related to the measuring current I . Using the relation between current and phase from the above Eqn. and rearranging to eliminate i we obtain an expression for I ,

$$I_c = 2i_c \left| \cos \pi \frac{\Phi_a}{\Phi_o} \cdot \sin \delta \right|$$

As $\sin \delta$ cannot be greater than unity we can obtain the critical measuring current, I_c from the above

$$I_c = 2i_c \left| \cos \pi \frac{\Phi_a}{\Phi_o} \right|$$

which gives a periodic dependence on the magnitude of the magnetic field, with a maximum when this field is an integer number of fluxons and a minimum at half integer values as shown in the below figure.

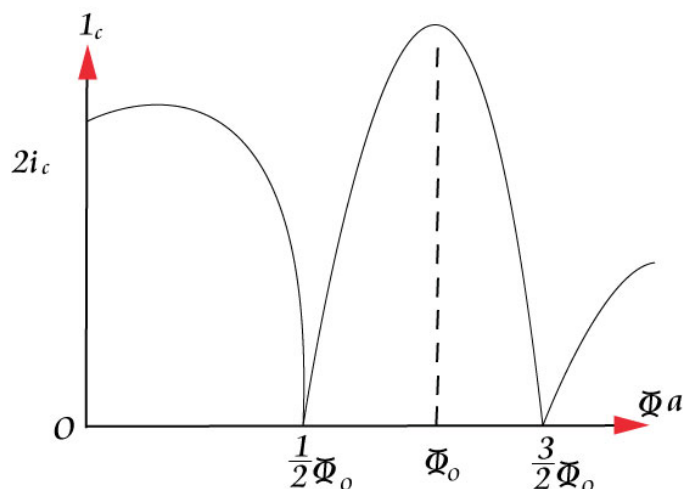


Figure 3.22: Critical measuring current, I_c , as a function of applied magnetic field. Adaped from J. Bland Thesis M. Phys (Hons)., 'A Mossbauer spectroscopy and magnetometry study of magnetic multilayers and oxides.' Oliver Lodge Labs, Dept. Physics, University of Liverpool.

3.1.2.8 Bibliography

- J. Bland, Thesis M. Phys (Hons)., 'A Mossbauer spectroscopy and magnetometry study of magnetic multilayers and oxides.' Oliver Lodge Labs, Dept. Physics, University of Liverpool.

- J. P. Cleuziou, W. Wernsdorfer, V. Bouchiat, T. Ondarçuhu, and M. Monthieux, *Nature Nanotech.*, 2006, **1**, 53.
- W. G. Jenksy, S. S. H. Sadeghiz, and J. P. Wikswo Jr., *J. Phys. D: Appl. Phys.*, 1997, **30**, 293.
- R. L. Fagaly, *Review of Scientific Instruments*, 2006, **77**, 101101.
- Quantum Design, Operating manual for the MPMS, 1999.

3.1.3 Practical Guide to Using a Superconducting Quantum Interference Device³

SQUIDs offer the ability to measure at sensitivities unachievable by other magnetic sensing methodologies. However, their sensitivity requires proper attention to cryogenics and environmental noise. SQUIDs should only be used when no other sensor is adequate for the task. There are many exotic uses for SQUID however we are just concerned with the laboratory applications of SQUID.

In most physical and chemical laboratories a device called a MPMS (Figure 3.23) is used to measure the magnetic moment of a sample by reading the output of the SQUID detector. In a MPMS the sample moves upward through the electronic pick up coils called gradiometers. One upward movement is one whole scan. Multiple scans are used and added together to improve measurement resolution. After collecting the raw voltages, there is computation of the magnetic moments of the sample.

The MPMS measures the moment of a sample by moving it through a liquid Helium cooled, superconducting sensing coil. Many different measurements can be carried out using an MPMS however we will discuss just a few.



Figure 3.23: A MPMS work station.

³This content is available online at <<http://cnx.org/content/m22968/1.2/>>.

3.1.3.1 Using an magnetic property measurement dystem (MPMS)

3.1.3.1.1 DC magnetization

DC magnetization is the magnetic per unit volume (M) of a sample. If the sample doesn't have a permanent magnetic moment, a field is applied to induce one. The sample is then stepped through a superconducting detection array and the SQUID's output voltage is processed and the sample moment computed. Systems can be configured to measure hysteresis loops, relaxation times, magnetic field, and temperature dependence of the magnetic moment.

A DC field can be used to magnetize samples. Typically, the field is fixed and the sample is moved into the detection coil's region of sensitivity. The change in detected magnetization is directly proportional to the magnetic moment of the sample. Commonly referred to as SQUID magnetometers, these systems are properly called SQUID susceptometers (Figure 3.24). They have a homogeneous superconducting magnet to create a very uniform field over the entire sample measuring region and the superconducting pickup loops. The magnet induces a moment allowing a measurement of magnetic susceptibility. The superconducting detection loop array is rigidly mounted in the center of the magnet. This array is configured as a gradient coil to reject external noise sources. The detection coil geometry determines what mathematical algorithm is used to calculate the net magnetization.

An important feature of SQUIDs is that the induced current is independent of the *rate* of flux change. This provides uniform response at all frequencies i.e., true dc response and allows the sample to be moved slowly without degrading performance. As the sample passes through a coil, it changes the flux in that coil by an amount proportional to the magnetic moment M of the sample. The peak-to-peak signal from a complete cycle is thus proportional to twice M . The SQUID sensor shielded inside a niobium can is located where the fringe fields generated by the magnet are less than 10 mT. The detection coil circuitry is typically constructed using NbTi (Figure 3.25). This allows measurements in applied fields of 9 T while maintaining sensitivities of 10^{-8} emu. Thermal insulation not shown is placed between the detection coils and the sample tube to allow the sample temperature to be varied.

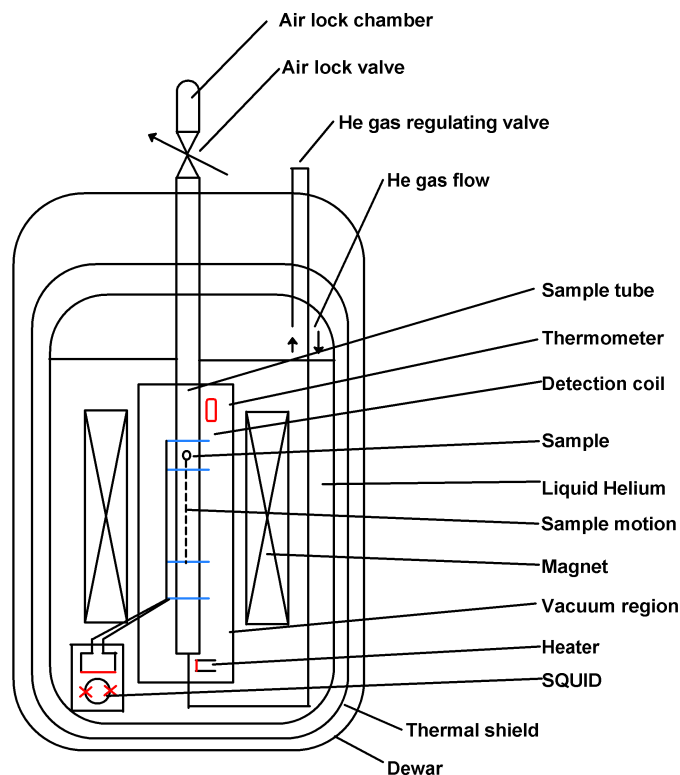


Figure 3.24: Schematic diagram of a MPMSR. Adapted from L. Fagaly, *Review of Scientific Instruments*, 2006, **77**, 101101.

The use of a variable temperature insert can allow measurements to be made over a wide range 1.8–400 K. Typically, the sample temperature is controlled by helium gas flowing slowly past the sample. The temperature of this gas is regulated using a heater located below the sample measuring region and a thermometer located above the sample region. This arrangement ensures that the entire region has reached thermal equilibrium prior to data acquisition. The helium gas is obtained from normal evaporation in the Dewar, and its flow rate is controlled by a precision regulating valve.

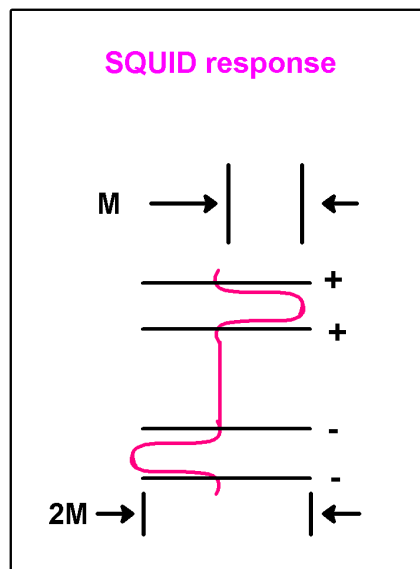


Figure 3.25: Signal output of an MPMS. Adapted from L. Fagaly, *Review of Scientific Instruments*, 2006, **77**, 101101.

3.1.3.2 Procedures when using an MPMS

3.1.3.2.1 Calibration

The magnetic moment calibration for the SQUID is determined by measuring a palladium standard over a range of magnetic fields and then by adjusting to obtain the correct moment for the standard. The palladium standard samples are effectively point sources with an accuracy of approximately 0.1%.

3.1.3.2.2 Sample mounting considerations

The type, size and geometry of a sample is usually sufficient to determine the method you use to attach it to the sample. However mostly for MPMS measurements a plastic straw is used. This is due to the straw having minimal magnetic susceptibility.

However there are a few important considerations for the sample holder design when mounting a sample for measurement in a magnetometer. The sample holder can be a major contributor to the background signal. Its contribution can be minimized by choosing materials with low magnetic susceptibility and by keeping the mass to a minimum such as a plastic straw mentioned above.

The materials used to hold a sample must perform well over the temperature range to be used. In a MPMS, the geometric arrangement of the background and sample is critical when their magnetic susceptibilities will be of similar magnitude. Thus, the sample holder should optimize the sample's positioning in the magnetometer. A sample should be mounted rigidly in order to avoid excess sample motion during measurement. A sample holder should also allow easy access for mounting the sample, and its background contribution should be easy to measure. This advisory introduces some mounting methods and discusses some of the more important considerations when mounting samples for the MPMS magnetometer. Keep in mind that these are only recommendations, not guaranteed procedures. The researcher is responsible for assuring that the methods and materials used will meet experimental requirements.

3.1.3.2.2.1 Sample Mounts

3.1.3.2.2.1.1 Platform mounting

For many types of samples, mounting to a platform is the most convenient method. The platform's mass and susceptibility should be as small as possible in order to minimize its background contribution and signal distortion.

3.1.3.2.2.1.2 Plastic disc

A plastic disc about 2 mm thick with an outside diameter equivalent to the pliable plastic tube's diameter (a clear drinking straw is suitable) is inserted and twisted into place. The platform should be fairly rigid. Mount samples onto this platform with glue. Place a second disc, with a diameter slightly less than the inside diameter of the tube and with the same mass, on top of the sample to help provide the desired symmetry. Pour powdered samples onto the platform and place a second disc on top. The powders will be able to align with the field. Make sure the sample tube is capped and ventilated.

3.1.3.2.2.1.3 Crossed threads

Make one of the lowest mass sample platforms by threading a cross of white cotton thread (colored dyes can be magnetic). Using a needle made of a nonmagnetic metal, or at least carefully cleaned, thread some white cotton sewing thread through the tube walls and tie a secure knot so that the thread platform is rigid. Glue a sample to this platform or use the platform as a support for a sample in a container. Use an additional thread cross on top to hold the container in place.

3.1.3.2.2.1.4 Gelatin capsule

Gelatin capsules can be very useful for containing and mounting samples. Many aspects of using gelatin capsules have been mentioned in the section, Containing the Sample. It is best if the sample is mounted near the capsule's center, or if it completely fills the capsule. Use extra capsule parts to produce mirror symmetry. The thread cross is an excellent way of holding a capsule in place.

3.1.3.2.2.1.5 Thread mounting

Another method of sample mounting is attaching the sample to a thread that runs through the sample tube. The thread can be attached to the sample holder at the ends of the sample tube with tape, for example. This method can be very useful with flat samples, such as those on substrates, particularly when the field is in the plane of the film. Be sure to close the sample tube with caps.

- Mounting with a disc platform.
- Mounting on crossed threads.
- Long thread mounting.

3.1.3.2.2.2 Steps for inserting the sample

1. Cut off a small section of a clear plastic drinking straw. The section must be small enough to fit inside the straw.
2. Weigh and measure the sample.
3. Use plastic tweezers to place the sample inside the small straw segment. It is important to use plastic tweezers not metallic ones as these will contaminate the sample.
4. Place the small straw segment inside the larger one. It should be approximately in the middle of the large drinking straw.
5. Attach the straw to the sample rod which is used to insert the sample into the SQUID machine.
6. Insert the sample rod with the attached straw into the vertical insertion hole on top of the SQUID.

3.1.3.2.3 Centre the sample

The sample must be centered in the SQUID pickup coils to ensure that all coils sense the magnetic moment of the sample. If the sample is not centered, the coils read only part of the magnetic moment.

During a centering measurement the MPMS scans the entire length of the samples vertical travel path, and the MPMS reads the maximum number of data points. During centering there are a number of terms which need to be understood.

1. A scan length is the length of a scan of a particular sample which should usually try and be the maximum of the sample.
2. A sample is centered when it is in the middle of a scan length. The data points are individual voltage readings plotting response curves in centering scan data files.
3. Autotracking is the adjustment of a sample position to keep a sample centered in SQUID coils. Auto-tracking compensates for thermal expansion and contraction in a sample rod.

As soon as a centering measurement is initiated, the sample transport moves upward, carrying the sample through the pickup coils. While the sample moves through the coils, the MPMS measures the SQUID's response to the magnetic moment of the sample and saves all the data from the centering measurement.

After a centering plot is performed the plot is examined to determine whether the sample is centered in the SQUID pickup coils. The sample is centered when the part of the large, middle curve is within 5cm of the half-way point of the scan length.

The shape of the plot is a function of the geometry of the coils. The coils are wound in a way which strongly rejects interference from nearby magnetic sources and lets the MPMS function without a superconducting shield around the pickup coils.

3.1.3.2.4 Geometric considerations

To minimize background noise and stray field effects, the MPMS magnetometer pick-up coil takes the form of a second-order gradiometer. An important feature of this gradiometer is that moving a long, homogeneous sample through it produces no signal as long as the sample extends well beyond the ends of the coil during measurement.

As a sample holder is moved through the gradiometer pickup coil, changes in thickness, mass, density, or magnetic susceptibility produce a signal. Ideally, only the sample to be measured produces this change. A homogeneous sample that extends well beyond the pick-up coils does not produce a signal, yet a small sample does produce a signal. There must be a crossover between these two limits. The sample length (along the field direction) should not exceed 10 mm. In order to obtain the most accurate measurements, it is important to keep the sample susceptibility constant over its length; otherwise distortions in the SQUID signal (deviations from a dipole signal) can result. It is also important to keep the sample close to the magnetometer centerline to get the most accurate measurements. When the sample holder background contribution is similar in magnitude to the sample signal, the relative positions of the sample and the materials producing the background are important. If there is a spatial offset between the two along the magnet axis, the signal produced by the combined sample and background can be highly distorted and will not be characteristic of the dipole moment being measured.

Even if the signal looks good at one temperature, a problem can occur if either of the contributions are temperature dependent.

Careful sample positioning and a sample holder with a center, or plane, of symmetry at the sample (i.e. materials distributed symmetrically about the sample, or along the principal axis for a symmetry plane) helps eliminate problems associated with spatial offsets.

3.1.3.2.5 Containing the Sample

Keep the sample space of the MPMS magnetometer clean and free of contamination with foreign materials. Avoid accidental sample loss into the sample space by properly containing the sample in an appropriate

sample holder. In all cases it is important to close the sample holder tube with caps in order to contain a sample that might become unmounted. This helps avoid sample loss and subsequent damage during the otherwise unnecessary recovery procedure. Position caps well out of the sample-measuring region and introduce proper venting.

3.1.3.2.6 Sample preparation workspace

Work area cleanliness and avoiding sample contamination are very important concerns. There are many possible sources of contamination in a laboratory. Use diamond tools when cutting hard materials. Avoid carbide tools because of potential contamination by the cobalt binder found in many carbide materials. The best tools for preparing samples and sample holders are made of plastic, titanium, brass, and beryllium copper (which also has a small amount of cobalt). Tools labeled non-magnetic can actually be made of steel and often be made "magnetic" from exposure to magnetic fields. However, the main concern from these "non-magnetic" tools is contamination by the iron and other ferrous metals in the tool. It is important to have a clean white-papered workspace and a set of tools dedicated to mounting your own samples. In many cases, the materials and tools used can be washed in dilute acid to remove ferrous metal impurities. Follow any acid washes with careful rinsing with deionized water.

Powdered samples pose a special contamination threat, and special precautions must be taken to contain them. If the sample is highly magnetic, it is often advantageous to embed it in a low susceptibility epoxy matrix like Duco cement. This is usually done by mixing a small amount of diluted glue with the powder in a suitable container such as a gelatin capsule. Potting the sample in this way can keep the sample from shifting or aligning with the magnetic field. In the case of weaker magnetic samples, measure the mass of the glue after drying and making a background measurement. If the powdered sample is not potted, seal it into a container, and watch it carefully as it is cycled in the airlock chamber.

3.1.3.2.7 Pressure equalization

The sample space of the MPMS has a helium atmosphere maintained at low pressure of a few torr. An airlock chamber is provided to avoid contamination of the sample space with air when introducing samples into the sample space. By pushing the purge button, the airlock is cycled between vacuum and helium gas three times, then pumped down to its working pressure. During the cycling, it is possible for samples to be displaced in their holders, sealed capsules to explode, and sample holders to be deformed. Many of these problems can be avoided if the sample holder is properly ventilated. This requires placing holes in the sample holder, out of the measuring region that will allow any closed spaces to be opened to the interlock chamber.

3.1.3.2.8 Air-sensitive samples and liquid samples

When working with highly air-sensitive samples or liquid samples it is best to first seal the sample into a glass tube. NMR and EPR tubes make good sample holders since they are usually made of a high-quality, low-susceptibility glass or fused silica. When the sample has a high susceptibility, the tube with the sample can be placed onto a platform like those described earlier. When dealing with a low susceptibility sample, it is useful to rest the bottom of the sample tube on a length of the same type of glass tubing. By producing near mirror symmetry, this method gives a nearly constant background with position and provides an easy method for background measurement (i.e., measure the empty tube first, then measure with a sample). Be sure that the tube ends are well out of the measuring region.

When going to low temperatures, check to make sure that the sample tube will not break due to differential thermal expansion. Samples that will go above room temperature should be sealed with a reduced pressure in the tube and be checked by taking the sample to the maximum experimental temperature prior to loading it into the magnetometer. These checks are especially important when the sample may be corrosive, reactive, or valuable.

3.1.3.2.9 Oxygen contamination

This application note describes potential sources for oxygen contamination in the sample chamber and discusses its possible effects. Molecular oxygen, which undergoes an antiferromagnetic transition at about 43 K, is strongly paramagnetic above this temperature. The MPMS system can easily detect the presence of a small amount of condensed oxygen on the sample, which when in the sample chamber can interfere significantly with sensitive magnetic measurements. Oxygen contamination in the sample chamber is usually the result of leaks in the system due to faulty seals, improper operation of the airlock valve, outgassing from the sample, or cold samples being loaded.

3.1.3.3 Bibliography

- J. Bland, Thesis M. Phys (Hons)., 'A Mossbauer spectroscopy and magnetometry study of magnetic multilayers and oxides.' Oliver Lodge Labs, Dept. Physics, University of Liverpool.
- Quantum Design, Operating manual for the MPMS, 1999.
- R. L. Fagaly, *Review of Scientific Instruments*, 2006, **77**, 101101.

3.2 IR Spectroscopy

3.2.1 IR Sample Preparation: A Practical Guide⁴

3.2.1.1 Introduction

Infrared spectroscopy is based on molecular vibrations caused by the oscillation of molecular dipoles. Bonds have characteristic vibrations depending on the atoms in the bond, the number of bonds and the orientation of those bonds with respect to the rest of the molecule. Thus, different molecules have specific spectra that can be collected for use in distinguishing products or identifying an unknown substance (to an extent.)

Collecting spectra through this method goes about one of three general ways. Nujol mulls and pressed pellets are typically used for collecting spectra of solids, while thin-film cells are used for solution-phase IR spectroscopy. Spectra of gases can also be obtained but will not be discussed in this guide.

3.2.1.2 Infrared optical materials and handling

While it is all well and wonderful that substances can be characterized in this fashion one still has to be able to hold the substances inside of the instrument and properly prepare the samples. In an infrared spectrometer (Figure 3.26) the sample to be analyzed is held in front of an infrared laser beam, in order to do this, the sample must be contained in something, consequently this means that the very container the sample is in will absorb some of the infrared beam.

⁴This content is available online at <<http://cnx.org/content/m43564/1.1/>>.

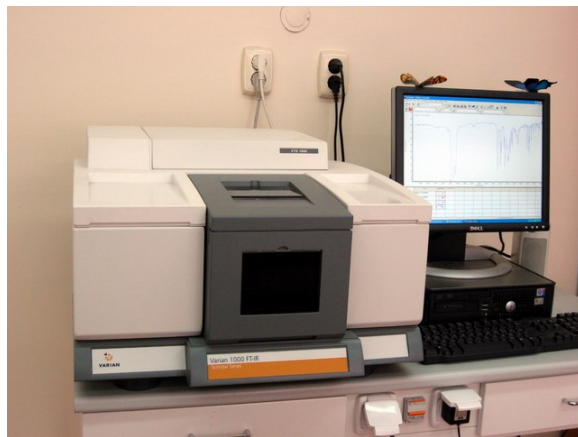


Figure 3.26: An example of a modern benchtop FT-IR spectrometer (Varian Corp.)

This is made somewhat complicated by the fact that all materials have some sort of vibration associated with them. Thus, if the sample holder has an optical window made of something that absorbs near where your sample does, the sample might not be distinguishable from the optical window of the sample holder. The range that is not blocked by a strong absorbance is known as a *window* (not to be confused with the optical materials of the cell.)

Windows are an important factor to consider when choosing the method to perform an analysis, as seen in Table 3.1 there are a number of different materials each with their own characteristic absorption spectra and chemical properties. Keep these factors in mind when performing analyses and precious sample will be saved. For most organic compounds NaCl works well though it is susceptible to attack from moisture. For metal coordination complexes KBr, or CsI typically work well due to their large windows. If money is not a problem then diamond or sapphire can be used for plates.

Material	Transparent Ranges (cm ⁻¹)	Solubility	Notes
NaCl	40,000 – 625	H ₂ O	Easy to polish, hygroscopic
Silica glass	55,000 – 3,000	HF	Attacked by HF
Quartz	40,000 – 2,500	HF	Attacked by HF
Sapphire	20,000 – 1,780	-	Strong
Diamond	40,000 – 2,500 and 1,800 - 200	-	Very strong, expensive, hard, useless for pellets.

continued on next page

CaF ₂	70,000 – 1,110	Acids	Attacked by acids, avoid ammonium salts.
BaF ₂	65,000 – 700	-	Avoid ammonium salts
ZnSe	10,000 – 550	Acids	Brittle, attacked by acids
AgCl	25,000 – 400	-	Soft, sensitive to light.
KCl	40,000 – 500	H ₂ O, Et ₂ O, acetone	
KBr	40,000 – 400	H ₂ O, EtOH	Hygroscopic, soft, easily polished, commonly used in making pellets.
CsBr	10,000 – 250	H ₂ O, EtOH, acetone	Hygroscopic, soft.
CsI	10,000 – 200	H ₂ O, EtOH, MeOH, acetone	Hygroscopic, soft.
Teflon	5,000 - 1,200, 1,200 - 900	-	Inert, disposable
Polyethylene	4,000 - 3,000, 2,800 - 1,460, 1,380 - 730, 720 - 30	-	Inert, disposable

Table 3.1: Various IR-transparent materials and their solubilities and other notes. M. R. Derrick, D. Stulik, and J. M. Landry, in *Scientific Tools in Conservation: Infrared Spectroscopy in Conservation Science*. Getty Conservation Institute (1999).

Proper handling of these plates will ensure they have a long, useful life. Here follows a few simple pointers on how to handle plates:

- Avoid contact with solvents that the plates are soluble in.
- Keep the plates in a dessicator, the less water the better, even if the plates are insoluble to water.
- Handle with gloves, clean gloves.
- Avoid wiping the plates to prevent scratching.

That said, these simple guidelines will likely reduce most damage that can occur to a plate by simply holding it other faults such as dropping the plate from a sufficient height can result in more serious damage.

3.2.1.3 Preparation of nujol mulls

A common method of preparing solid samples for IR analysis is mulling. The principle here is by grinding the particles to below the wavelength of incident radiation that will be passing through there should be limited scattering. To suspend those tiny particles, an oil, often referred to as Nujol is used. IR-transparent salt plates are used to hold the sample in front of the beam in order to acquire data. To prepare a sample for IR analysis using a salt plate, first decide what segment of the frequency band should be studied, refer to Table 3.1 for the materials best suited for the sample. Figure 3.27 shows the materials needed for preparing a mull.



Figure 3.27: In this photograph, the sample, ferrocene, two clean and polished KBr plates, an agate mortar and pestle, a mounting card and a spatula are displayed as the base minimum requirements for preparing a sample through a Nujol mull. Of course, a small bottle of mineral oil is also necessary.

Preparing the mull is performed by taking a small portion of sample and adding approximately 10% of the sample volume worth of the oil and grinding this in an agate mortar and pestle as demonstrated in Figure 3.28. The resulting mull should be transparent with no visible particles.



Figure 3.28: Mulling ferrocene into mineral oil with a mortar and pestle.

Another method involves dissolving the solid in a solvent and allowing it to dry in the agate pestle. If using this method ensure that all of the solvent has evaporated since the solvent bands will appear in the spectrum. Some gentle heating may assist this process. This method creates very fine particles that are of a relatively consistent size. After addition of the oil further mixing (or grinding) may be necessary.

Plates should be stored in a desiccator to prevent erosion by atmospheric moisture and should appear roughly transparent. Some materials such as silicon will not, however. Gently rinse the plates with hexanes to wash any residual material off of the plates. Removing the plates from the desiccator and cleaning them should follow the preparation of the mull in order to maintain the integrity of the salt plates. Of course, if the plate is not soluble in water then it is still a good idea just to prevent the threat of mechanical trauma or a stray jet of acetone from a wash bottle.

Once the mull has been prepared, add a drop to one IR plate (Figure 3.29), place the second plate on top of the drop and give it a quarter turn in order to evenly coat the plate surface as seen in Figure 3.30. Place it into the spectrometer and acquire the desired data.

NOTE: Always handle with gloves and preferably away from any sinks, faucets, or other sources of running or spraying water.



Figure 3.29: The prepared mull from an agate mortar and pestle being applied to a polished KBr plate.



Figure 3.30: Sandwiched KBr plates with a Nujol mull of ferrocene.

NOTE: Spectra acquired by this method will have strong C-H absorption bands throughout several ranges $3,000 - 2,800 \text{ cm}^{-1}$ and $1,500 - 1,300 \text{ cm}^{-1}$ and may obscure signal.

Cleaning the plate is performed as previously mentioned with hexanes or chloroform can easily be performed by rinsing and leaving them to dry in the hood. Place the salt plates back into the desiccator as soon as reasonably possible to prevent damage. It is highly advisable to polish the plates after use, no scratches, fogging, or pits should be visible on the face of the plate. Chips, so long as they don't cross the center of the plate are survivable but not desired. The samples of damaged salt plates in Figure 3.31 show common problems associated with use or potentially mishandling. Clouding, and to an extent, scratches can be polished out with an iron rouge. Areas where the crystal lattice is disturbed below the surface are impossible to fix and chips cannot be reattached.

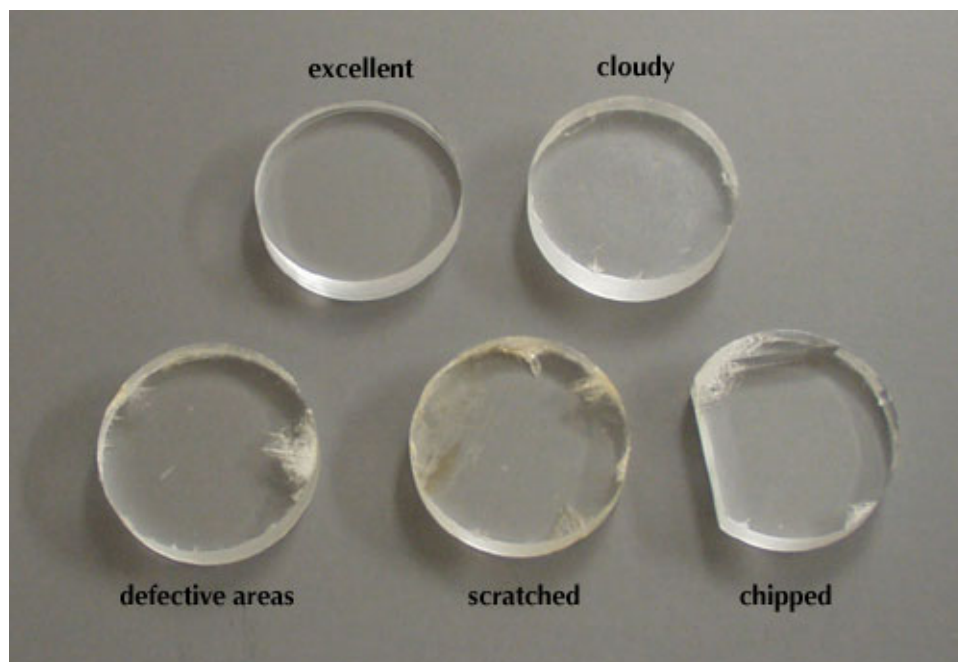


Figure 3.31: A series of plates indicating various forms of physical damage with a comparison to a good plate (Copyright: Colorado University-Boulder).

3.2.1.4 Preparation of pellets

In an alternate method, this technique is along the same lines of the nujol mull except instead of the suspending medium being mineral oil, the suspending medium is a salt. The solid is ground into a fine powder with an agate mortar and pestle with an amount of the suspending salt. Preparing pellets with diamond for the suspending agent is somewhat illadvised considering the great hardness of the substance. Generally speaking, an amount of KBr or CsI is used for this method since they are both soft salts. Two approaches can be used to prepare pellets, one is somewhat more expensive but both usually yield decent results.

The first method is the use of a press. The salt is placed into a cylindrical holder and pressed together with a ram such as the one seen in (Figure 3.32). Afterwards, the pellet, in the holder, is placed into the instrument and spectra acquired.



Figure 3.32: A large benchtop hydraulic press (Specac Inc.)

An alternate, and cheaper method requires the use of a large hex nut with a 0.5 inch inner diameter, two bolts, and two wrenches such as the kit seen in Figure 3.33. Step-by-step instructions for loading and using the press follows:

1. Screw one of the bolts into the nut about half way.
2. Place the salt pellet mixture into the other opening of the nut and level by tapping the assembly on a countertop.
3. Screw in the second bolt and place the assembly on its side with the bolts parallel to the countertop. Place one of the wrenches on the bolt on the right side with the handle aiming towards yourself.
4. Take the second wrench and place it on the other bolt so that it attaches with an angle from the table of about 45 degrees.
5. The second bolt is tightened with a body weight and left to rest for several minutes. Afterwards, the bolts are removed, and the sample placed into the instrument.



Figure 3.33: A simple pellet press with cell holder. (Cole-Parmer)

Some pellet presses also have a vacuum barb such as the one seen in (Figure 3.33). If your pellet press has one of these, consider using it as it will help remove air from the salt pellet as it is pressed. This ensures a more uniform pellet and removes absorbances in the collected spectrum due to air trapped in the pellet.

3.2.1.5 Preparation of solution cells

Solution cells (Figure 3.34) are a handy way of acquiring infrared spectra of compounds in solution and is particularly handy for monitoring reactions.



Figure 3.34: A sealed solution cell with two injection ports and a schematic of its construction (Perkin-Elmer Inc.)

A thin-film cell consists of two salt plates with a very thin space in between them (Figure 3.35). Two channels allow liquid to be injected and then subsequently removed. The windows on these cells can be made from a variety of IR optical materials. One particularly useful one for water-based solutions is CaF_2 as it is not soluble in water.

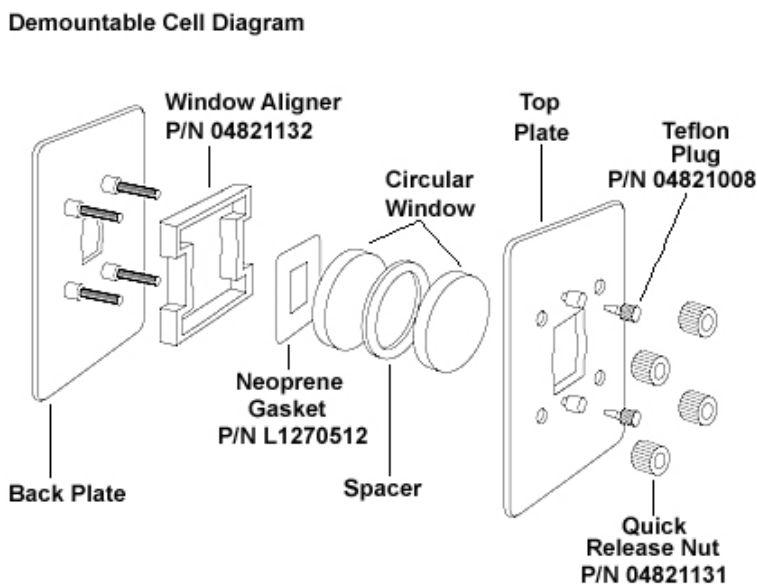


Figure 3.35: A sealed solution cell with two injection ports and a schematic of its construction (Perkin-Elmer Inc.).

Cleaning these cells can be performed by removing the solution, flushing with fresh solvent and gently removing the solvent by syringe. Do not blow air or nitrogen through the ports as this can cause mechanical deformation in the salt window if the pressure is high enough.

3.2.1.6 Deuterated solvent effects

One of the other aspects to solution-phase IR is that the solvent utilized in the cell has a characteristic absorption spectra. In some cases this can be alleviated by replacing the solvent with its deuterated sibling. The benefit here is that C-H bonds are now C-D bonds and have lower vibrational frequencies. Compiled in Figure 3.36 is a set of common solvents.

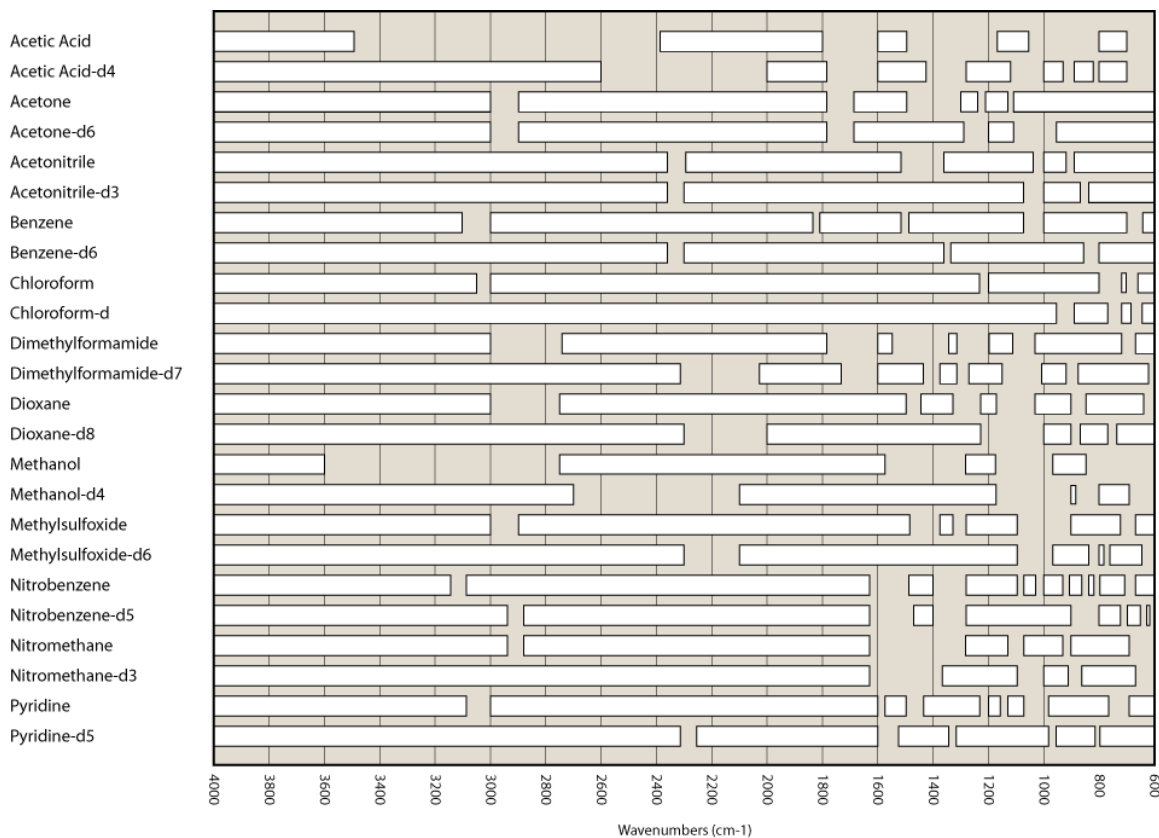


Figure 3.36: IR transparencies of various solvents and their heavy counterparts. Adapted from N. L. McNiven and R. Court, *Appl. Spectrosc.*, 1970, **24**, 296.

This effect has numerous benefits and is often applied to determining what vibrations correspond to what bond in a given molecular sample. This is often accomplished by using isotopically labeled “heavy” reagents such as ones that contain ^2H , ^{15}N , ^{18}O , or ^{13}C .

3.2.1.7 Basic troubleshooting

There are numerous problems that can arise from improperly prepared samples, this section will go through some of the common problems and how to correct them. For this demonstration, spectra of ferrocene will be used. The molecular structure and a photograph of the brightly colored organometallic compound are shown in Figure 3.37 and Figure 3.38.

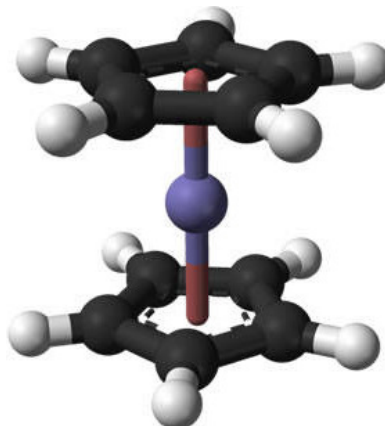


Figure 3.37: Structure of ferrocene ($\text{Fe}(\text{C}_5\text{H}_5)_2$).



Figure 3.38: Image of ferrocene powder ($\text{Fe}(\text{C}_5\text{H}_5)_2$).

Figure 3.39 illustrates what a good sample of ferrocene looks like prepared in a KBr pellet. The peaks are well defined and sharp. No peak is flattened at 0% transmittance and Christiansen scattering is not evident in the baseline.

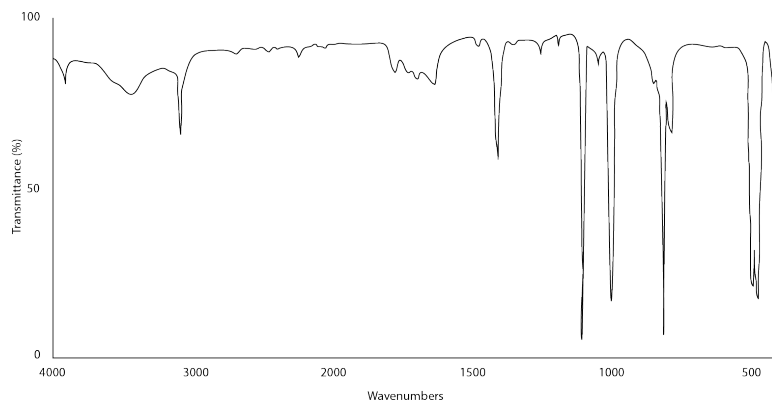


Figure 3.39: A good spectrum of ferrocene in a KBr Pellet. Adapted from NIST Chemistry WebBook.

Figure 3.40 illustrates a sample with some peaks with intensities that are saturated and lose resolution making peak-picking difficult. In order to correct for this problem, scrape some of the sample off of the salt plate with a rubber spatula and reseal the opposite plate. By applying a thinner layer of sample one can improve the resolution of strongly absorbing vibrations.

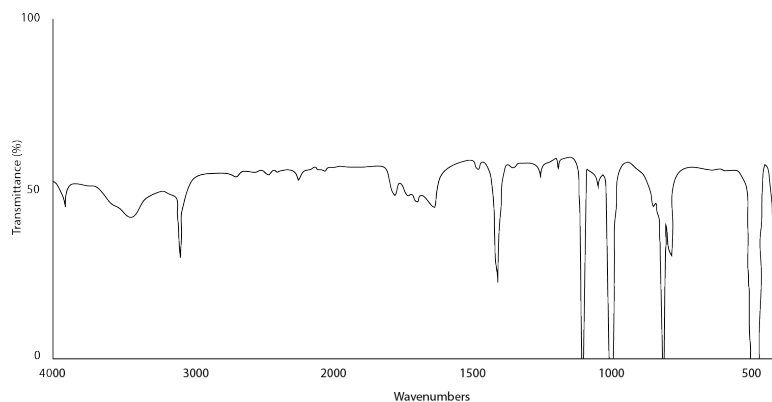


Figure 3.40: An overly concentrated sample of ferrocene in a KBr pellet. Adapted from NIST Chemistry WebBook.

Figure 3.41 illustrates a sample in which too much mineral oil was added to the mull so that the C-H bonds are far more intense than the actual sample. This can be remedied by removing the sample from the plate, grinding more sample and adding a smaller amount of the mull to the plate. Another possible way of doing this is if the sample is insoluble in hexanes, add a little to the mull and wick away the hexane-oil

mixture to leave a dry solid sample. Apply a small portion of oil and replate.

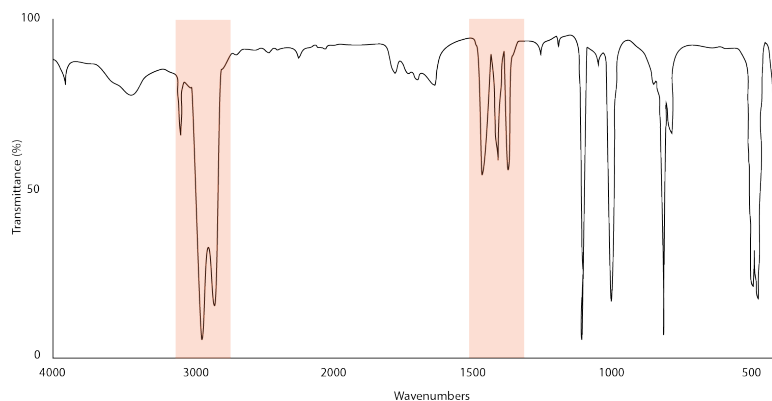


Figure 3.41: A spectrum illustrating the problems of using Nujol, areas highlighted in orange are absorbances related to the addition of Nujol to a sample. Notice how in the 1500 wavenumber region the addition of the Nujol has partially occulted the absorbance by the ferrocene. Adapted from NIST Chemistry WebBook.

Figure 3.42 illustrates the result of particles being too large and scattering light. To remedy this, remove the mull and grind further or else use the solvent deposition technique described earlier.

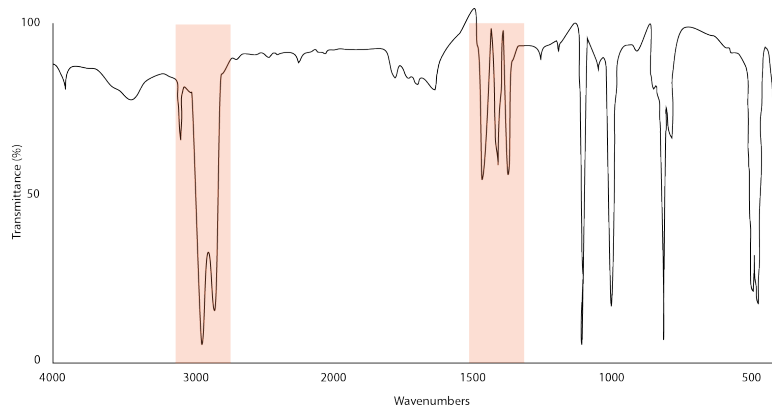


Figure 3.42: A sample exhibiting the Christiansen effect on ferrocene in a Nujol mull. Orange boxes indicate Nujol occult ranges. Adapted from NIST Chemistry WebBook.

3.2.1.8 Bibliography

- N. L. McNiven and R. Court, *Appl. Spectrosc.*, 1970, **24**, 296.

- M. R. Derrick, D. Stulik, and J. M. Landry, in *Scientific Tools in Conservation: Infrared Spectroscopy in Conservation Science*. Getty Conservation Institute, Los Angeles (1999).
- D. L. Pavia, G. M. Lampman, and G. S. Kriz, in *Introduction to Spectroscopy: A Guide for Students of Organic Chemistry*. Harcourt Brace College Publishers, Fort Worth (1996).

3.2.2 Characteristic IR Vibrational Modes for Hydrocarbon Compounds⁵

Functional group	Mode	Wavenumber range (cm ⁻¹)
CH ₃	Asymmetric stretch	2962±10
CH ₃	Symmetric stretch	2872±10
CH ₃	Asymmetric bend	1460±10
CH ₃	Symmetric bend (umbrella mode)	1375±10
CH ₂	Asymmetric stretch	2926±10
CH ₂	Symmetric stretch	2855±10
CH ₂	Scissors	1455±10
CH ₂	Rock	720±10
CH	Stretch	~2900 (weak)
CH	Bend	~1350 (weak)

Table 3.2: Stretching and bending bands for alkanes.

Substitution	C-H stretch (cm ⁻¹)	C=C stretch (cm ⁻¹)	Out of plane bend (cm ⁻¹)
Vinyl	3090 – 3075	1660 - 1630	990±5, 910±5
Vinylidene	3090 – 3075	1660 - 1630	890±5
<i>Cis</i>	3050 – 3000	1660 - 1630	690±10
<i>Trans</i>	3050 – 3000	1680 - 1665	965±5
Tri-substituted	3050 – 3000	1680 - 1665	815±25
Tetra-substituted	-	1680 - 1665	-

Table 3.3: The stretching bands for alkenes.

Substitution	C-H stretch (cm ⁻¹)	C≡C stretch (cm ⁻¹)	C-H wag (cm ⁻¹)
Mono-substituted	3350 – 3250	2140 – 2100	700 - 600
Di-substituted	-	2260 - 2190	-

Table 3.4: The stretching bands for alkynes.

⁵This content is available online at <<http://cnx.org/content/m34623/1.1/>>.

Substitution	Out-of-plane C-H bending (cm^{-1})	Ring bend (cm^{-1})
Mono	770 – 710	690±10
Ortho	810 - 750	-
Meta	770 - 735	690±10
Para	860 – 790	-

Table 3.5: Bands for mono- and di-substituted benzene rings.

Vibration	Wavenumber (cm^{-1})
CH ₃ symmetric stretch	2925±5
CH ₃ bend overtone	2865±5

Table 3.6: Bands for methyl groups bonded to benzene rings.

3.2.3 Fourier Transform Infrared Spectroscopy of Metal Ligand Complexes⁶

3.2.3.1 Introduction

The infrared (IR) range of the electromagnetic spectrum is usually divided into three regions:

- The far-infrared is always used for rotational spectroscopy, with wavenumber range 400 – 10 cm^{-1} and lower energy.
- The mid-infrared is suitable for a detection of the fundamental vibrations and associated rotational-vibrational structure with the frequency range approximately 4000 – 400 cm^{-1} .
- The near-Infrared with higher energy and wave number range 14000 – 4000 cm^{-1} , can excite overtone or higher harmonic vibrations.

For classical light material interaction theory, if a molecule can interact with an electromagnetic field and absorb a photon of certain frequency, the transient dipole of molecular functional group must oscillate at that frequency. Correspondingly, this transition dipole moment must be a non-zero value, however, some special vibration can be IR inactive for the stretching motion of a homonuclear diatomic molecule and vibrations do not affect the molecule's dipole moment (e.g., N₂).

3.2.3.2 Mechanistic description of the vibrations of polyatomic molecules

A molecule can vibrate in many ways, and each way is called a "vibrational mode". If a molecule has N atoms, linear molecules have 3N-5 degrees of vibrational modes whereas nonlinear molecules have 3N-6 degrees of vibrational modes. Take H₂O for example; a single molecule of H₂O has O-H bending mode (Figure 3.43a), antisymmetric stretching mode (Figure 3.43b), and symmetric stretching mode (Figure 3.43c).

⁶This content is available online at <<http://cnx.org/content/m34660/1.1/>>.

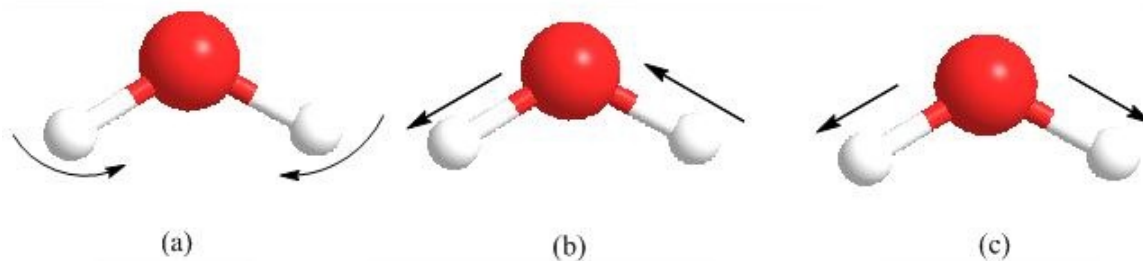


Figure 3.43: Three types of hydroxy vibration modes. (a) bending mode; (b) antisymmetric stretching mode; (c) symmetric stretching mode.

If a diatomic molecule has a harmonic vibration with the energy, (3.1), where $n+1/2$ with $n = 0, 1, 2 \dots$. The motion of the atoms can be determined by the force equation, (3.2), where k is the force constant). The vibration frequency can be described by (3.3). In which m is actually the reduced mass (m_{red} or μ), which is determined from the mass m_1 and m_2 of the two atoms, (3.4).

$$E_n = -h\nu \quad (3.1)$$

$$F = -kx \quad (3.2)$$

$$\omega = (k/m)^{1/2} \quad (3.3)$$

$$m_{\text{red}} = \mu = \frac{m_1 m_2}{m_1 + m_2} \quad (3.4)$$

3.2.3.3 Principle of absorption bands

In IR spectrum, absorption information is generally presented in the form of both wavenumber and absorption intensity or percent transmittance. The spectrum is generally showing wavenumber (cm^{-1}) as the x-axis and absorption intensity or percent transmittance as the y-axis.

Transmittance, "T", is the ratio of radiant power transmitted by the sample (I) to the radiant power incident on the sample (I_0). Absorbance (A) is the logarithm to the base 10 of the reciprocal of the transmittance (T). The absorption intensity of molecule vibration can be determined by the Lambert-Beer Law, (3.5). In this equation, the transmittance spectra ranges from 0 to 100%, and it can provide clear contrast between intensities of strong and weak bands. Absorbance ranges from infinity to zero. The absorption of molecules can be determined by several components. In the absorption equation, ϵ is called molar extinction coefficient, which is related to the molecule behavior itself, mainly the transition dipole moment, c is the concentration of the sample, and l is the sample length. Line width can be determined by the interaction with surroundings.

$$A = \log(1/T) = -\log(I/I_0) = \epsilon cl \quad (3.5)$$

3.2.3.4 The infrared spectrometer

As shown in Figure 3.44, there are mainly four parts for fourier transform infrared spectrometer (FTIR):

- **Light source.** Infrared energy is emitted from a glowing black-body source as continuous radiations.
- **Interferometer.** It contains the interferometer, the beam splitter, the fixed mirror and the moving mirror. The beam splitter takes the incoming infrared beam and divides it into two optical beams. One beam reflects off the fixed mirror. The other beam reflects off of the moving mirror which moves a very short distance. After the divided beams are reflected from the two mirrors, they meet each other again at the beam splitter. Therefore, an interference pattern is generated by the changes in the relative position of the moving mirror to the fixed mirror. The resulting beam then passes through the sample and is eventually focused on the detector.
- **Sample compartment.** It is the place where the beam is transmitted through the sample. In the sample compartment, specific frequencies of energy are absorbed.
- **Detector.** The beam finally passes to the detector for final measurement. The two most popular detectors for a FTIR spectrometer are deuterated triglycine sulfate (pyroelectric detector) and mercury cadmium telluride (photon or quantum detector). The measured signal is sent to the computer where the Fourier transformation takes place.

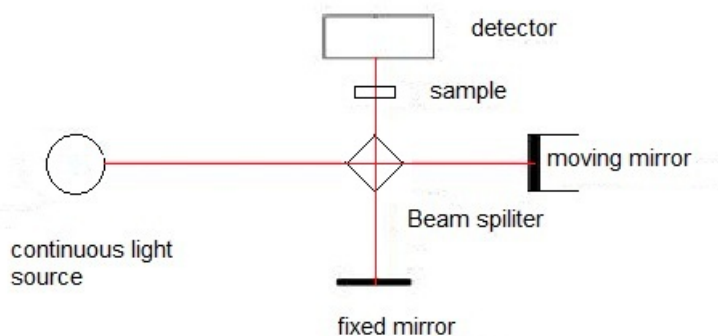


Figure 3.44: The main components of a fourier transform infrared (FTIR) spectrometer.

3.2.3.5 A typical application: the detection of metal ligand complexes

3.2.3.5.1 Some general absorption peaks for common types of functional groups

It is well known that all molecules chemicals have distinct absorption regions in the IR spectrum. Table 3.7 shows the absorption frequencies of common types of functional groups. For systematic evaluation, the IR spectrum is commonly divided into some sub-regions.

- In the region of $4000 - 2000 \text{ cm}^{-1}$, the appearance of absorption bands usually comes from stretching vibrations between hydrogen and other atoms. The O-H and N-H stretching frequencies range from $3700 - 3000 \text{ cm}^{-1}$. If hydrogen bond forms between O-H and other group, it generally caused peak line shape broadening and shifting to lower frequencies. The C-H stretching bands occur in the region of

3300 - 2800 cm^{-1} . The acetylenic C-H exhibits strong absorption at around 3300 cm^{-1} . Alkene and aromatic C-H stretch vibrations absorb at 3200-3000 cm^{-1} . Generally, asymmetric vibrational stretch frequency of alkene C-H is around 3150 cm^{-1} , and symmetric vibrational stretch frequency is between 3100 cm^{-1} and 3000 cm^{-1} . The saturated aliphatic C-H stretching bands range from 3000 - 2850 cm^{-1} , with absorption intensities that are proportional to the number of C-H bonds. Aldehydes often show two sharp C-H stretching absorption bands at 2900 - 2700 cm^{-1} . However, in water solution, C-H vibrational stretch is much lower than in non-polar solution. It means that the strong polarity solution can greatly reduce the transition dipole moment of C-H vibration.

- Furthermore, the stretching vibrations frequencies between hydrogen and other heteroatoms are between 2600 - 2000 cm^{-1} , for example, S-H at 2600 - 2550 cm^{-1} , P-H at 2440 - 2275 cm^{-1} , Si-H at 2250 - 2100 cm^{-1} .
- The absorption bands at the 2300 - 1850 cm^{-1} region usually present only from triple bonds, such as $\text{C}\equiv\text{C}$ at 2260 - 2100 cm^{-1} , $\text{C}\equiv\text{N}$ at 2260 - 2000 cm^{-1} , diazonium salts $-\text{N}\equiv\text{N}$ at approximately 2260 cm^{-1} , allenes $\text{C}=\text{C}=\text{C}$ at 2000 - 1900 cm^{-1} . The peaks of these groups are all have strong absorption intensities. The 1950 - 1450 cm^{-1} region stands for double-bonded functional groups vibrational stretching.
- Most carbonyl $\text{C}=\text{O}$ stretching bands range from 1870 - 1550 cm^{-1} , and the peak intensities are from mean to strong. Conjugation, ring size, hydrogen bonding, and steric and electronic effects can lead to significant shifts in absorption frequencies. Furthermore, if carbonyl links with electron-withdrawing group, such as acid chlorides and acid anhydrides, it would give rise to IR bands at 1850 - 1750 cm^{-1} . Ketones usually display stretching bands at 1715 cm^{-1} .
- None conjugated aliphatic $\text{C}=\text{C}$ and $\text{C}=\text{N}$ have absorption bands at 1690 - 1620 cm^{-1} . Besides, around 1430 and 1370 cm^{-1} , there are two identical peaks presenting C-H bending.
- The region from 1300 - 910 cm^{-1} always includes the contributions from skeleton C-O and C-C vibrational stretches, giving additional molecular structural information correlated with higher frequency areas. For example, ethyl acetate not only shows its carbonyl stretch at 1750 - 1735 cm^{-1} , but also exhibits its identical absorption peaks at 1300 - 1000 cm^{-1} from the skeleton vibration of C-O and C-C stretches.

Group	Frequency (cm^{-1})	Strength appearance
C-H stretch	2850 - 3400	Strong in nonpolar solvent Weak in polar solvent
O-H stretch N-H stretch	3200 - 3700	Broad in solvent
$\text{C}\equiv\text{N}$ stretch R-N=C=S stretch	2050 - 2300	Medium or strong
$\text{C}\equiv\text{O}$ stretch (bound with metal)	around 2000	Medium or strong
$\text{C}\equiv\text{C}$ stretch	2100 - 2260	Weak
$\text{C}=\text{O}$ stretch	ca 1715 (ketone), ca 1650 (amides)	Strong
$\text{C}=\text{C}$ stretch	1450 - 1700	Weak to strong
<i>continued on next page</i>		

C-H bend	1260 - 1470	Strong
C-O stretch	1040 - 1300	Medium or strong

Table 3.7: The typical frequencies of functional groups.

3.2.3.5.2 General introduction of metal ligand complex

The metal electrons fill into the molecular orbital of ligands (CN, CO, etc.) to form complex compound. As shown in Figure 3.45, a simple molecular orbital diagram for CO can be used to explain the binding mechanism.

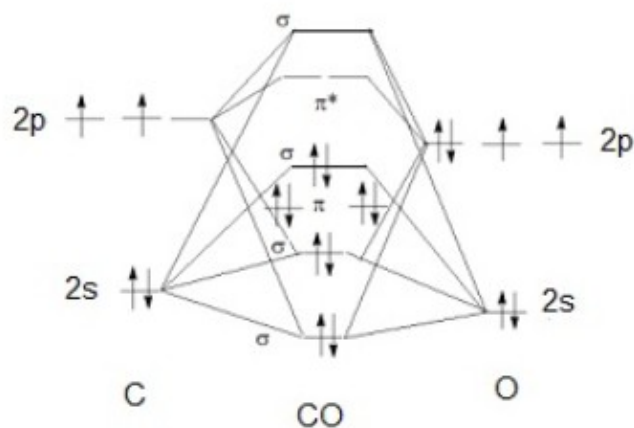


Figure 3.45: Molecular orbital diagram for carbon monoxide (CO).

The CO and metal can bind with three ways:

- Donation of a pair of electrons from the C-O σ^* orbital into an empty metal orbital (Figure 3.46a).
- Donation from a metal d orbital into the C-O π^* orbital to form a M-to-CO π -back bond (Figure 3.46b).
- Under some conditions a pair of carbon π electron can donate into an empty metal d-orbital.

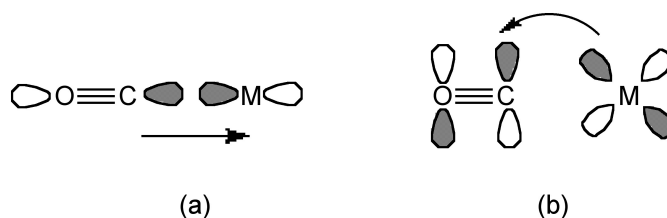


Figure 3.46: Main binding interaction types between metal and CO. (a) CO-to-metal σ bond; (b) M-to-CO π -back bond.

3.2.3.5.3 Some factors to influence the band shifts and strength

Herein, we mainly consider two properties: ligand stretch frequency and their absorption intensity. Take the ligand CO for example again. The frequency shift of the carbonyl peaks in the IR mainly depends on the bonding mode of the CO (terminal or bridging) and electron density on the metal. The intensity and peak numbers of the carbonyl bands depends on some factors: CO ligands numbers, geometry of the metal ligand complex and fermi resonance.

3.2.3.5.3.1 Effect on electron density on metal

As shown in Table 3.8, a greater charge on the metal center result in the CO stretches vibration frequency decreasing. For example, $[\text{Ag}(\text{CO})]^+$ show higher frequency of CO than free CO, which indicates a strengthening of the CO bond. σ donation removes electron density from the nonbonding HOMO of CO. From Figure 3.45, it is clear that the HOMO has a small amount of anti-bonding property, so removal of an electron actually increases (slightly) the CO bond strength. Therefore, the effect of charge and electronegativity depends on the amount of metal to CO π -back bonding and the CO IR stretching frequency.

d^x	Complex	νCO stretch frequency (cm^{-1})
	free CO	2143
d^{10}	$[\text{Ag}(\text{CO})]^+$	2204
d^{10}	$\text{Ni}(\text{CO})_4$	2060
d^{10}	$[\text{Co}(\text{CO})_4]^-$	1890
d^6	$[\text{Mn}(\text{CO})_6]^+$	2090
d^6	$\text{Cr}(\text{CO})_6$	2000
d^6	$[\text{V}(\text{CO})_6]^-$	1860

Table 3.8: Different types of ligands frequencies of different electron density on a metal center.

If the electron density on a metal center is increasing, more π -back bonding to the CO ligand(s) will also increase, as shown in Table 3.8. It means more electron density would enter into the empty carbonyl π^* orbital and weaken the C-O bond. Therefore, it makes the M-CO bond strength increasing and more double-bond-like ($\text{M}=\text{C}=\text{O}$).

3.2.3.5.3.2 Ligand donation effect

Some cases, as shown in Table 3.9, different ligands would bind with same metal at the same metal-ligand complex. For example, if different electron density groups bind with $\text{Mo}(\text{CO})_3$ as the same form, as shown in Figure 3.47, the CO vibrational frequencies would depend on the ligand donation effect. Compared with the PPh_3 group, CO stretching frequency which the complex binds the PF_3 group (2090, 2055 cm^{-1}) is higher. It indicates that the absolute amount of electron density on that metal may have certain effect on the ability of the ligands on a metal to donate electron density to the metal center. Hence, it may be explained by the Ligand donation effect. Ligands that are *trans* to a carbonyl can have a large effect on the ability of the CO ligand to effectively π -backbond to the metal. For example, two *trans* π -backbonding ligands will partially compete for the same d-orbital electron density, weakening each other's net M-L π -backbonding. If the *trans* ligand is a π -donating ligand, the free metal to CO π -backbonding can increase the M-CO bond strength (more M=C=O character). It is well known that pyridine and amines are not those strong π -donors. However, they are even worse π -backbonding ligands. So the CO is actually easy for π -back donation without any competition. Therefore, it naturally reduces the CO IR stretching frequencies in metal carbonyl complexes for the ligand donation effect.

Metal Ligand Complex	CO stretch frequency (cm^{-1})
$\text{Mo}(\text{CO})_3(\text{PF}_3)_3$	2090, 2055
$\text{Mo}(\text{CO})_3[\text{P}(\text{OMe})_3]_3$	1977, 1888
$\text{Mo}(\text{CO})_3(\text{PPh}_3)_3$	1934, 1835
$\text{Mo}(\text{CO})_3(\text{NCCH}_3)_3$	1915, 1783
$\text{Mo}(\text{CO})_3(\text{pyridine})_3$	1888, 1746

Table 3.9: The effect of different types of ligands on the frequency of the carbonyl ligand.

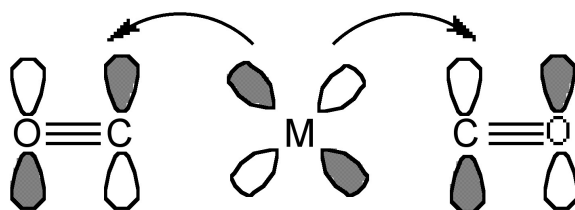


Figure 3.47: Schematic representation of competitive back-donation from a transition metal to multiple π -acceptor ligands

3.2.3.5.3.3 Geometry effects

Some cases, metal-ligand complex can form not only terminal but also bridging geometry. As shown in Figure 3.48, in the compound $\text{Fe}_2(\text{CO})_7(\text{dipy})$, CO can act as a bridging ligand. Evidence for a bridging mode of coordination can be easily obtained through IR spectroscopy. All the metal atoms bridged by a carbonyl can donate electron density into the π^* orbital of the CO and weaken the CO bond, lowering vibration frequency of CO. In this example, the CO frequency in terminal is around 2080 cm^{-1} , and in bridge, it shifts to around 1850 cm^{-1} .

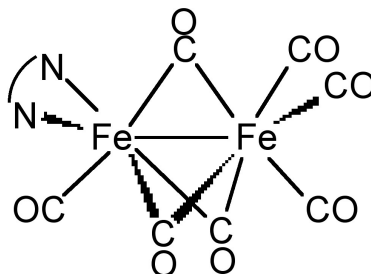


Figure 3.48: The structure of $\text{Fe}_2(\text{CO})_7(\text{dipy})$.

3.2.3.6 Bibliography

- *Introduction of Fourier Transform Infrared Spectrometry*, Thermo Nicolet Corporation (2001).
- C. P. S. Hsu, *Handbook of Instrumental Techniques for Analytical Chemistry*. Prentice-Hall, NJ (1997).
- B. E. Douglas, D. H. McDaniel, and J. J. Alexander, *Concepts and Models of Inorganic Chemistry*, 3rd Ed., John Wiley & Sons, Winchester (1994).
- A. F. Cotton and M. J. Troup, *J. Am. Chem. Soc.*, 1974, **96**, 1233.
- K. Nakamoto. *Infrared and Raman Spectra of Inorganic and Coordination Compounds*, 3rd ed., Wiley, New York (1978).

3.2.4 Pump-probe Detection of Molecular Functional Group Vibrational Lifetime⁷

3.2.4.1 Introduction

The dynamics of molecular functional group plays an important role during a chemical process, chemical bond forming and breaking, energy transfer and other dynamics happens within picoseconds domain. It is very difficult to study such fast processes directly, for decades scientists can only learn from theoretical calculations, lacking experimental methods.

However, with the development of ultrashort pulsed laser enable experimental study of molecular functional group dynamics. With ultrafast laser technologies, people develop a series of measuring methods, among which, pump-probe technique is widely used to study the molecular functional group dynamics. Here we concentrate on how to use pump-probe experiment to measure functional group vibrational lifetime. The principle, experimental setup and data analysis will be introduced.

3.2.4.2 Principles of the pump-probe technique

For every function group within a molecule, such as the $\text{C}\equiv\text{N}$ triple bond in phenyl selenocyanate ($\text{C}_6\text{H}_5\text{SeCN}$) or the C-D single bond in deuterated chloroform (DCCl_3), they have an individual infrared vibrational mode and associated energy levels. For a typical 3-level system (Figure 3.49), both the 0 to 1 and the 1 to 2 transition are near the probe pulse frequency (they don't necessarily need to have exactly the same frequency).

⁷This content is available online at <<http://cnx.org/content/m34610/1.2/>>.

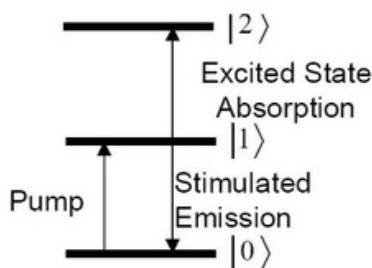


Figure 3.49: Schematic representation of a typical three level system.

In a pump-probe experiment, we use the geometry as is shown in Figure 3.50. Two synchronized laser beams, one of which is called pump beam (E_{pu}) while the other probe beam (E_{pr}). There is a delay in time between each pulse. The laser pulses hit the sample, the intensity of ultrafast laser (fs or ps) is strong enough to generate 3rd order polarization and produce 3rd order optical response signal which is used to give dynamics information of molecular function groups. For the total response signals we have (3.6), where μ_{10} , μ_{21} are transition dipole moment and E_0 , E_1 , and E_2 are the energies of the three levels, and t_3 is the time delay between pump and probe beam. The delay t_3 is varied and the response signal intensity is measured. The functional group vibration life time is determined from the data.

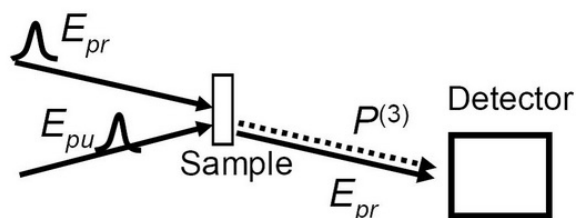


Figure 3.50: The geometry of the pump-probe experiment.

$$S = 4\mu_{10}^4 e^{-i(E_1-E_0)t_3/\hbar-\Gamma t_3} - 2\mu_{10}^2 \mu_{21}^2 e^{-i(E_1-E_0)t_3/\hbar-\Gamma t_3} \quad (3.6)$$

3.2.4.3 Typical experimental set-up

The optical layout of a typical pump-probe setup is schematically displayed in Figure 3.51. In the setup, the output of the oscillator (500 mW at 77 MHz repetition rate, 40 nm bandwidth centered at 800 nm) is split into two beams (1:4 power ratio). Of this, 20% of the power is to seed a femtosecond (fs) amplifier whose output is 40 fs pulses centered at 800 nm with power of ~ 3.4 W at 1 KHz repetition rate. The rest (80%) of the seed goes through a bandpass filter centered at 797.5 nm with a width of 0.40 nm to seed a picosecond (ps) amplifier. The power of the stretched seed before entering the ps amplifier cavity is only ~ 3 mW. The

output of the ps amplifier is 1ps pulses centered at 800 nm with a bandwidth ~ 0.6 nm. The power of the ps amplifier output is ~ 3 W. The fs amplifier is then to pump an optical parametric amplifier (OPA) which produces ~ 100 fs IR pulses with bandwidth of ~ 200 cm^{-1} that is tunable from 900 to 4000 cm^{-1} . The power of the fs IR pulses is 7 \sim 40 mW, depending on the frequencies. The ps amplifier is to pump a ps OPA which produces ~ 900 fs IR pulses with bandwidth of ~ 21 cm^{-1} , tunable from 900 - 4000 cm^{-1} . The power of the fs IR pulses is 10 \sim 40 mW, depending on frequencies.

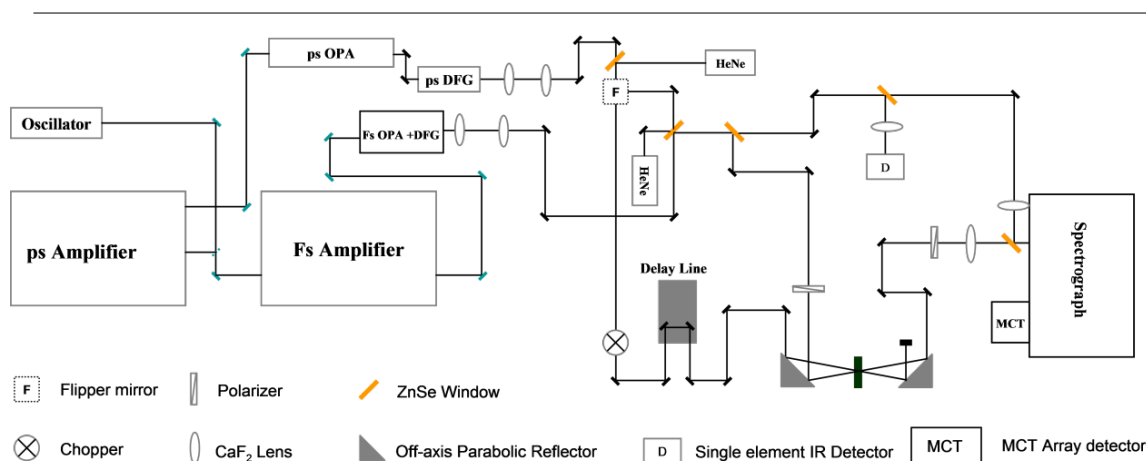


Figure 3.51: Schematic representation of the optical layout for a pump-probe experiment.

In a typical pump-probe setup, the ps IR beam is collimated and used as the pump beam. Approximately 1% of the fs IR OPA output is used as the probe beam whose intensity is further modified by a polarizer placed before the sample. Another polarizer is placed after the sample and before the spectrograph to select different polarizations of the signal. The signal is then sent into a spectrograph to resolve frequency, and detected with a mercury cadmium telluride (MCT) dual array detector. Use of a pump pulse (femtosecond, wide band) and a probe pulse (picoseconds, narrow band), scanning the delay time and reading the data from the spectrometer, will give the lifetime of the functional group. The wide band pump and spectrometer described here is for collecting multiple group of pump-probe combination.

3.2.4.3.1 Data analysis

For a typical pump-probe curve shown in Figure 3.52 life time t is defined as the corresponding time value to the half intensity as time zero.

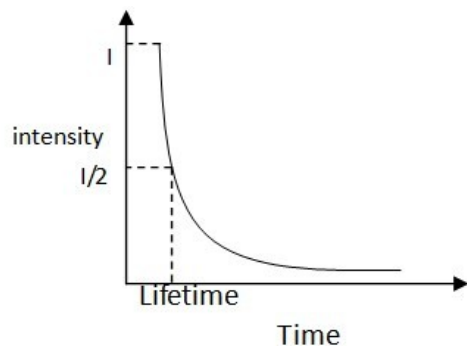


Figure 3.52: A typical pump-probe curve.

Table 3.10 shows the pump-probe data of the $\text{C}\equiv\text{N}$ triple bond in a series of aromatic cyano compounds: *n*-propyl cyanide ($\text{C}_3\text{H}_7\text{CN}$), ethyl thiocyanate ($\text{C}_2\text{H}_5\text{SCN}$), and ethyl selenocyanate ($\text{C}_2\text{H}_5\text{SeCN}$) for which the $\nu_{\text{C}\equiv\text{N}}$ for each compound (measured in CCl_4 solution) is 2252 cm^{-1} , 2156 cm^{-1} , and $\sim 2155\text{ cm}^{-1}$, respectively.

Delay (ps)	$\text{C}_3\text{H}_7\text{CN}$	$\text{C}_2\text{H}_5\text{SCN}$	$\text{C}_2\text{H}_5\text{SeCN}$
0	-0.00695	-0.10918	-0.06901
0.1	-0.0074	-0.10797	-0.07093
0.2	-0.00761	-0.1071	-0.07247
0.3	-0.00768	-0.10545	-0.07346
0.4	-0.0076	-0.10487	-0.07429
0.5	-0.00778	-0.10287	-0.07282
0.6	-0.00782	-0.10286	-0.07235
0.7	-0.00803	-0.10222	-0.07089
0.8	-0.00764	-0.10182	-0.07073
0.9	-0.00776	-0.10143	-0.06861
1	-0.00781	-0.10099	-0.06867
1.1	-0.00745	-0.10013	-0.06796
<i>continued on next page</i>			

1.2	-0.00702	-0.10066	-0.06773
1.3	-0.00703	-0.0989	-0.06767
1.4	-0.00676	-0.0995	-0.06638
1.5	-0.00681	-0.09757	-0.06691
1.6	-0.00639	-0.09758	-0.06696
1.7	-0.00644	-0.09717	-0.06583
1.8	-0.00619	-0.09741	-0.06598
1.9	-0.00613	-0.09723	-0.06507
2	-0.0066	-0.0962	-0.06477
2.5	-0.00574	-0.09546	-0.0639
3	-0.0052	-0.09453	-0.06382
3.5	-0.00482	-0.09353	-0.06389
4	-0.0042	-0.09294	-0.06287
4.5	-0.00387	-0.09224	-0.06197
5	-0.00351	-0.09009	-0.06189
5.5	-0.00362	-0.09084	-0.06188
6	-0.00352	-0.08938	-0.06021
6.5	-0.00269	-0.08843	-0.06028
7	-0.00225	-0.08788	-0.05961
7.5	-0.00231	-0.08694	-0.06065
8	-0.00206	-0.08598	-0.05963
8.5	-0.00233	-0.08552	-0.05993
9	-0.00177	-0.08503	-0.05902
9.5	-0.00186	-0.08508	-0.05878
10	-0.00167	-0.0842	-0.0591
11	-0.00143	-0.08295	-0.05734

Table 3.10: Pump-probe intensity data for C≡N stretching frequency in *n*-propyl cyanide, ethyl thiocyanate, and ethyl selenocyanate as a function of delay (ps).

A plot of intensity versus time for the data from TABLE is shown Figure 3.53. From these curves the C≡N stretch lifetimes can be determined for C₃H₇CN, C₂H₅SCN, and C₂H₅SeCN as ~5.5 ps, ~84 ps, and ~282 ps, respectively.

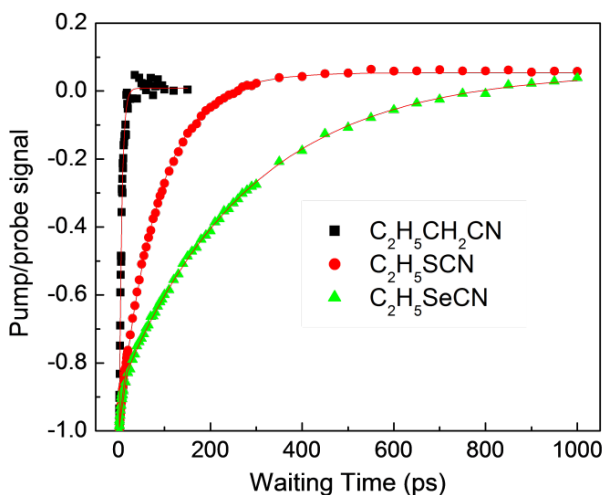


Figure 3.53: The $C\equiv N$ stretch lifetimes for benzyl cyanide, phenyl thiocyanate, and phenyl selenocyanate.

From what is shown above, the pump-probe method is used in detecting $C\equiv N$ vibrational lifetimes in different chemicals. One measurement only takes several second to get all the data and the lifetime, showing that pump-probe method is a powerful way to measure functional group vibrational lifetime.

3.3 Raman Spectroscopy

3.3.1 Raman and Surface-Enhanced Raman Spectroscopy⁸

3.3.1.1 What is Raman spectroscopy?

Raman spectroscopy is a powerful tool for determining chemical species. As with other spectroscopic techniques, Raman spectroscopy detects certain interactions of light with matter. In particular, this technique exploits the existence of Stokes and Anti-Stokes scattering to examine molecular structure. When radiation in the near infrared (NIR) or visible range interacts with a molecule, several types of scattering can occur. Three of these can be seen in the energy diagram in Figure 3.54.

⁸This content is available online at <http://cnx.org/content/m34528/1.1/>.

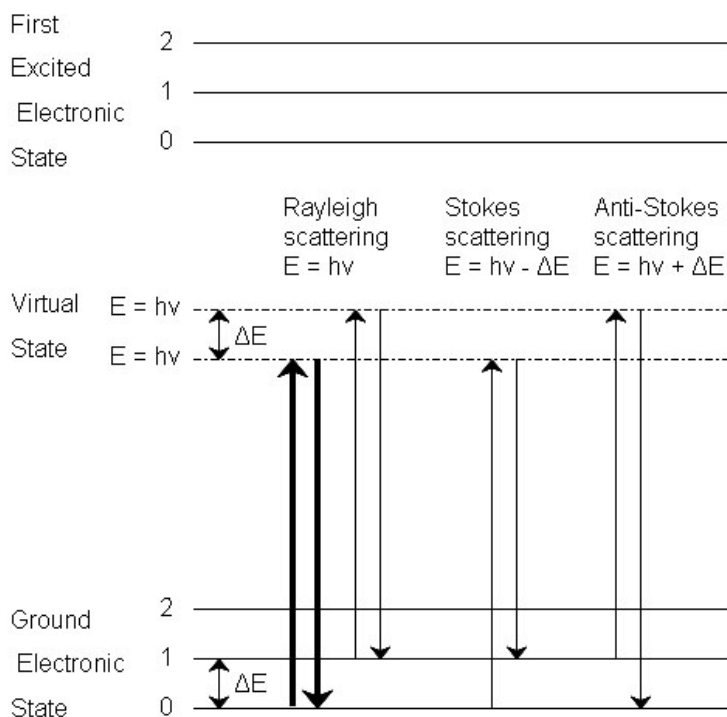


Figure 3.54: Three types of scattering by a molecule excited by a photon with energy $E = h\nu$. The most common transition is marked with bold arrows.

In all three types of scattering, an incident photon of energy $h\nu$ raises the molecule from a vibrational state to one of the infinite number of virtual states located between the ground and first electronic states. The type of scattering observed is dependent on how the molecule relaxes after excitation.

Rayleigh scattering

- Step 1. The molecule is excited to any virtual state.
- Step 2. The molecule relaxes back to its original state.
- Step 3. The photon is scattered elastically, leaving with its original energy.

Stokes scattering

- Step 1. The molecule is excited to any virtual state.
- Step 2. The molecule relaxes back to a higher vibrational state than it had originally.
- Step 3. The photon leaves with energy $h\nu - \Delta E$ and has been scattered inelastically.

Anti-Stokes scattering

- Step 1. The molecule begins in a vibrationally excited state.
- Step 2. The molecule is excited to any virtual state.
- Step 3. The molecule relaxes back to a lower vibrational state than it had originally.
- Step 4. The photon leaves with energy $h\nu + \Delta E$, and has been scattered superelastically.

Rayleigh scattering is by far the most common transition, due to the fact that no change has to occur in the vibrational state of the molecule. The anti-Stokes transition is the least common, as it requires the molecule to be in a vibrationally excited state before the photon is incident upon it. Due to the lack of intensity of the anti-Stokes signal and filtering requirements that eliminate photons with incident energy and higher, generally only Stokes scattering is used in Raman measurements. The relative intensities of Rayleigh, Stokes and anti-Stokes scattering can be seen in Figure 3.55.

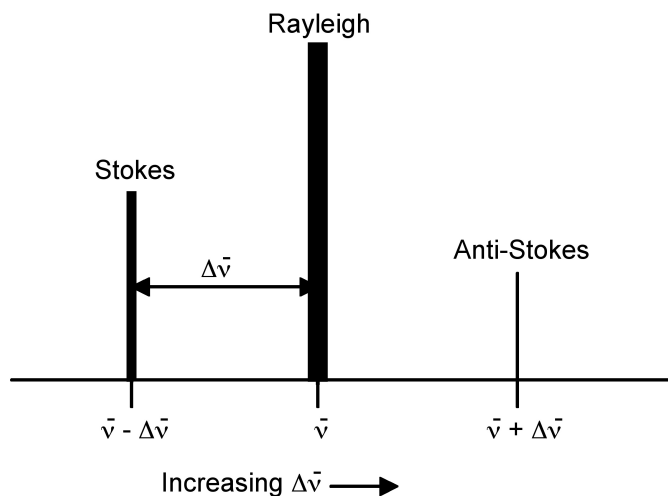


Figure 3.55: Location and relative intensity (indicated by peak height and width) of the Stokes and anti-Stokes scattering relative to Rayleigh scattering.

Raman spectroscopy observes the change in energy between the incident and scattered photons associated with the Stokes and anti-Stokes transitions. This is typically measured as the change in the wavenumber (cm^{-1}), from the incident light source. Because Raman measures the change in wavenumber, measurements can be taken using a source at any wavelength; however, near infrared and visible radiation are commonly used. Photons with ultraviolet wavelengths could work as well, but tend to cause photodecomposition of the sample.

3.3.1.2 Comparison between Raman and infrared spectroscopy

Raman spectroscopy sounds very much like infrared (IR) spectroscopy; however, IR examines the wavenumber at which a functional group has a vibrational mode, while Raman observes the shift in vibration from an incident source. The Raman frequency shift is identical to the IR peak frequency for a given molecule or functional group. As mentioned above, this shift is independent of the excitation wavelength, giving versatility to the design and applicability of Raman instruments.

The cause of the vibration is also mechanistically different between IR and Raman. This is because the two operate on different sets of selection rules. IR absorption requires a dipole moment or change in charge distribution to be associated with the vibrational mode. Only then can photons of the same energy as the vibrational state of molecule interact. A schematic of this can be seen in Figure 3.56.



Figure 3.56: A change in dipole moment is required for a vibrational mode to be IR active.

Raman signals, on the other hand, due to scattering, occur because of a molecule's polarizability, illustrated in Figure 3.57. Many molecules that are inactive or weak in the IR will have intense Raman signals. This results in often complementary techniques.

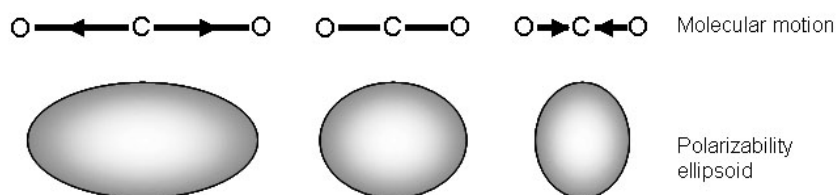


Figure 3.57: A change in the polarizability of a bond is required for a vibrational mode to be Raman active.

3.3.1.3 What does Raman spectroscopy measure?

Raman activity depends on the polarizability of a bond. This is a measure of the deformability of a bond in an electric field. This factor essentially depends on how easy it is for the electrons in the bond to be displaced, inducing a temporary dipole. When there is a large concentration of loosely held electrons in a bond, the polarizability is also large, and the group or molecule will have an intense Raman signal. Because of this, Raman is typically more sensitive to the molecular framework of a molecule rather than a specific functional group as in IR. This should not be confused with the polarity of a molecule, which is a measure of the separation of electric charge within a molecule. Polar molecules often have very weak Raman signals due to the fact that electronegative atoms hold electrons so closely.

Raman spectroscopy can provide information about both inorganic and organic chemical species. Many electron atoms, such as metals in coordination compounds, tend to have many loosely bound electrons, and therefore tend to be Raman active. Raman can provide information on the metal ligand bond, leading to knowledge of the composition, structure, and stability of these complexes. This can be particularly useful in metal compounds that have low vibrational absorption frequencies in the IR. Raman is also very useful for determining functional groups and fingerprints of organic molecules. Often, Raman vibrations are highly characteristic to a specific molecule, due to vibrations of a molecule as a whole, not in localized groups. The groups that do appear in Raman spectra have vibrations that are largely localized within the group, and often have multiple bonds involved.

3.3.1.4 What is surface-enhanced Raman spectroscopy?

Raman measurements provide useful characterization of many materials. However, the Raman signal is inherently weak (less than 0.001% of the source intensity), restricting the usefulness of this analytical tool. Placing the molecule of interest near a metal surface can dramatically increase the Raman signal. This is the basis of surface-enhanced Raman spectroscopy (SERS). There are several factors leading to the increase in Raman signal intensity near a metal surface.

1. The distance to the metal surface.
 - Signal enhancement drops off with distance from the surface.
 - The molecule of interest must be close to the surface for signal enhancement to occur.
2. Details about the metal surface: morphology and roughness.
 - This determines how close and how many molecules can be near a particular surface area.
3. The properties of the metal.
 - Greatest enhancement occurs when the excitation wavelength is near the plasma frequency of the metal.
4. The relative orientation of the molecule to the normal of the surface.
 - The polarizability of the bonds within the molecule can be affected by the electrons in the surface of the metal.

3.3.1.5 Bibliography

- W. Demtröder, *Laser Spectroscopy Basic Concepts and Instrumentation*, Springer, New York (2003).
- D. W. Mayo, F. A. Miller, and R. W. Hannah, *Course Notes on the Interpretation of Infrared and Raman Spectra*, Wiley-VCH, Hoboken, NJ (2003).
- D. A. Skoog, F. J. Holler, and S. R. Crouch, *Principles of Instrumental Analysis*, 6th edition, Brooks Cole (2006).

3.3.2 Surface-Enhanced Raman Spectroscopy for the Study of Surface Chemistry⁹

The ever-rising interest in nanotechnology involves the synthesis and application of materials with a very high surface area to volume ratio. This places increasing importance on understanding the chemistry occurring at a surface, particularly the surface of a nanoparticle. Slight modifications of the nanoparticle or its surrounding environment can greatly affect many properties including the solubility, biological toxicity, and reactivity of the nanomaterial. Noble metal nanomaterials are of particular interest due to their unique optical properties and biological inertness.

One tool employed to understand the surface chemistry of noble metal nanomaterial, particularly those composed of gold or silver is *surface-enhanced Raman spectroscopy* (SERS). Replacing a metal surface with a metal nanoparticle increases the available surface area for the adsorption of molecules. Compared to a flat metal surface, a similar sample size using nanoparticles will have a dramatically stronger signal, since signal intensity is directly related to the concentration of the molecule of interest. Due to the shape and size of the structure, the electrons in the nanoparticle oscillate collectively when exposed to incident electromagnetic radiation. This is called the *localized surface plasmon resonance* (LSPR) of the nanoparticle. The LSPR of the nanoparticles boosts the Raman signal intensity dramatically for molecules of interest near the surface of the nanoparticle. In order to maximize this effect, a nanoparticle should be selected with its resonant wavelength falling in the middle of the incident and scattered wavelengths.

The overall intensity enhancement of SERS can be as large as a factor of 10^6 , with the surface plasmon resonance responsible for roughly four orders of magnitude of this signal increase. The other two orders of

⁹This content is available online at <<http://cnx.org/content/m34522/1.1/>>.

magnitude have been attributed to chemical enhancement mechanisms arising charge interactions between the metal particle and the adsorbate or from resonances in the adsorbate alone, as discussed above.

3.3.2.1 Why is SERS useful for studying surface chemistry?

Traditionally, SERS uses nanoparticles made of conductive materials, such as gold, to learn more about a particular molecule. However, of interest in many growing fields that incorporate nanotechnology is the structure and functionalization of a nanoparticle stabilized by some surfactant or capping agent. In this case, SERS can provide valuable information regarding the stability and surface structure of the nanoparticle. Another use of nanoparticles in SERS is to provide information about a ligand's structure and the nature of ligand binding. In many applications it is important to know whether a molecule is bound to the surface of the nanoparticle or simply electrostatically interacting with it.

3.3.2.2 Sample preparation and instrumental details

The standard Raman instrument is composed of three major components. First, the instrument must have an illumination system. This is usually composed of one or more lasers. The major restriction for the illumination system is that the incident frequency of light must not be absorbed by the sample or solvent. The next major component is the sample illumination system. This can vary widely based on the specifics of the instrument, including whether the system is a standard macro-Raman or has micro-Raman capabilities. The sample illumination system will determine the phase of material under investigation. The final necessary piece of a Raman system is the spectrometer. This is usually placed 90° away from the incident illumination and may include a series of filters or a monochromator. An example of a macro-Raman and micro-Raman setup can be seen in Figure 3.58 and Figure 3.59. A macro-Raman spectrometer has a spatial resolution anywhere from $100\ \mu\text{m}$ to one millimeter while a micro-Raman spectrometer uses a microscope to magnify its spatial resolution.

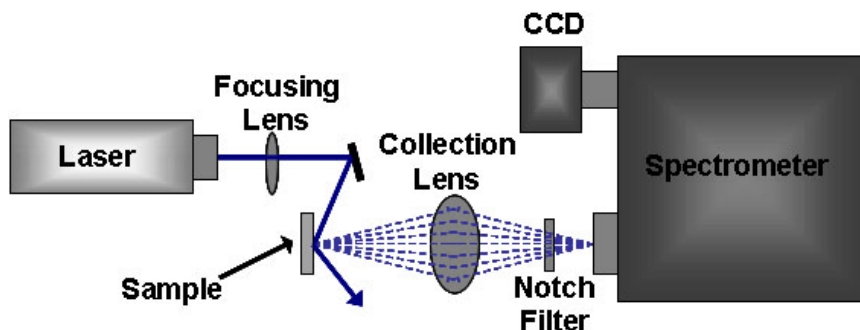


Figure 3.58: Schematic of a macro-Raman spectrometer.

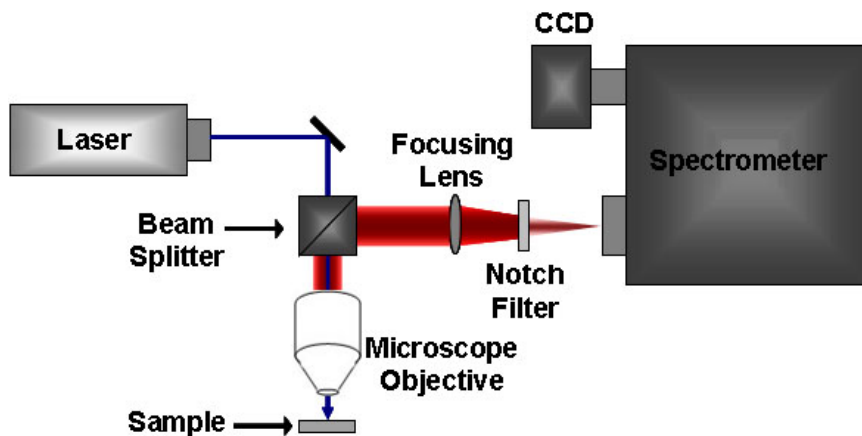


Figure 3.59: Schematic of a micro-Raman spectrometer where illumination and collection are performed through microscope objective.

3.3.2.3 Bibliography

- D. A. Skoog, F. J. Holler, and S. R. Crouch, *Principles of Instrumental Analysis*, 6th Ed, Brooks Cole (2006).
- P. L. Stiles, J. A. Dieringer, N. C. Shah, and R. P. van Duyne, *Annu. Rev. Anal. Chem.*, 2008, **1**, 601.

3.3.3 Characterization of Single-Walled Carbon Nanotubes by Raman Spectroscopy¹⁰

3.3.3.1 Introduction

Carbon nanotubes (CNTs) have proven to be a unique system for the application of Raman spectroscopy, and at the same time Raman spectroscopy has provided an exceedingly powerful tool useful in the study of the vibrational properties and electronic structures of CNTs. Raman spectroscopy has been successfully applied for studying CNTs at single nanotube level.

The large van der Waals interactions between the CNTs lead to an agglomeration of the tubes in the form of bundles or ropes. This problem can be solved by wrapping the tubes in a surfactant or functionalizing the SWNTs by attaching appropriate chemical moieties to the sidewalls of the tube. Functionalization causes a local change in the hybridization from sp^2 to sp^3 of the side-wall carbon atoms, and Raman spectroscopy can be used to determine this change. In addition information on length, diameter, electronic type (metallic or semiconducting), and whether nanotubes are separated or in bundle can be obtained by the use of Raman spectroscopy. Recent progress in understanding the Raman spectra of single walled carbon nanotubes (SWNT) have stimulated Raman studies of more complicated multi-wall carbon nanotubes (MWNT), but unfortunately quantitative determination of the latter is not possible at the present state of art.

¹⁰This content is available online at <<http://cnx.org/content/m22925/1.2/>>.

3.3.3.2 Characterizing SWNTs

Raman spectroscopy is a single resonance process, i.e., the signals are greatly enhanced if either the incoming laser energy (E_{laser}) or the scattered radiation matches an allowed electronic transition in the sample. For this process to occur, the phonon modes are assumed to occur at the center of the Brillouin zone ($q = 0$). Owing to their one dimensional nature, the Π -electronic density of states of a perfect, infinite, SWNTs form sharp singularities which are known as van Hove singularities (vHs), which are energetically symmetrical with respect to Fermi level (E_f) of the individual SWNTs. The allowed optical transitions occur between matching vHs of the valence and conduction band of the SWNTs, i.e., from first valence band vHs to the first conduction band vHs (E_{11}) or from the second vHs of the valence band to the second vHs of the conduction band (E_{22}). Since the quantum state of an electron (k) remains the same during the transition, it is referred to as k -selection rule.

The electronic properties, and therefore the individual transition energies in SWNTs are given by their structure, i.e., by their chiral vector that determines the way SWNT is rolled up to form a cylinder. Figure 3.60 shows a SWNT having vector R making an angle θ , known as the chiral angle, with the so-called zigzag or r_1 direction.

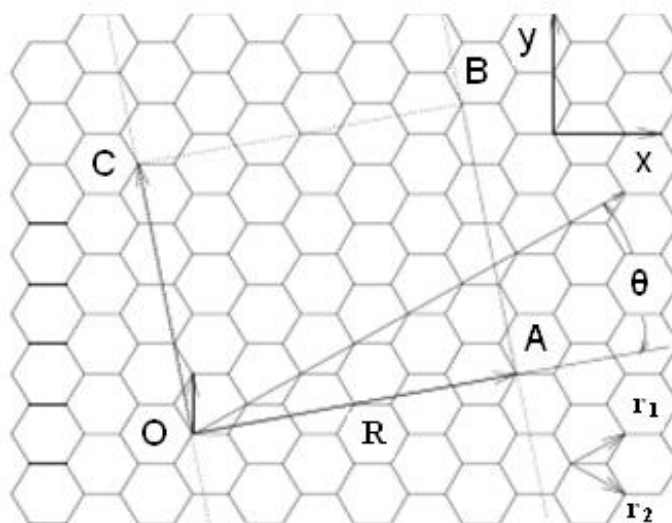


Figure 3.60: The unrolled honeycomb lattice of a nanotube. When the sites O and A, and the sites B and C are connected, a portion of a graphene sheet can be rolled seamlessly to form a SWNT. The vectors OA and OB define the chiral vector R of the nanotube, respectively. The rectangle OABC defines the unit cell if the nanotube. The figure is constructed for $(n,m) = (4,2)$ nanotube. Adapted from M. S. Dresselhaus, G. Dresselhaus, R. Saito, and A. Jorio, *Physics Reports*, 2004, **2**, 47.

Raman spectroscopy of an ensemble of many SWNTs having different chiral vectors is sensitive to the subset of tubes where the condition of allowed transition is fulfilled. A ‘Kataura-Plot’ gives the allowed electronic transition energies of individual SWNTs as a function of diameter d , hence information on which tubes are resonant for a given excitation wavelength can be inferred. Since electronic transition energies vary roughly as $1/d$, the question whether a given laser energy probes predominantly semiconducting or metallic tubes depends on the mean diameter and diameter distribution in the SWNT ensemble. However,

the transition energies that apply to an isolated SWNT do not necessarily hold for an ensemble of interacting SWNTs owing to the mutual van der Waals interactions.

Figure 3.61 shows a typical Raman spectrum from 100 to 3000 cm^{-1} taken of SWNTs produced by catalytic decomposition of carbon monoxide (HiPco-process). The two dominant Raman features are the radial breathing mode (RBM) at low frequencies and tangential (G-band) multifeature at higher frequencies. Other weak features, such as the disorder induced D-band and the G' band (an overtone mode) are also shown.

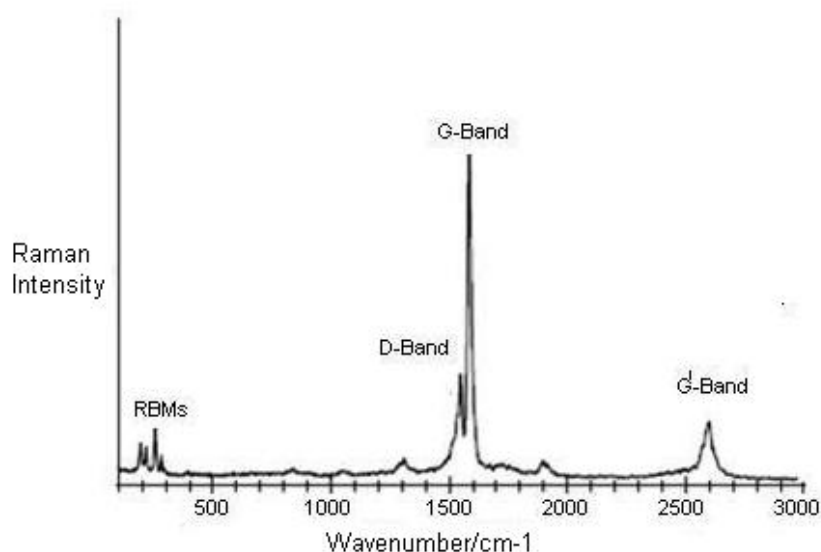


Figure 3.61: Raman spectrum of HiPco SWNTs using a laser of wavelength of $\lambda_{\text{exc}} = 633$ nm. Adapted from R. Graupner, *J. Raman Spectrosc.*, 2007, **38**, 673.

3.3.3.3 Modes in the Raman spectra of SWNTs

3.3.3.3.1 Radial breathing modes (RBMs)

Out of all Raman modes observed in the spectra of SWNTs, the radial breathing modes are unique to SWNTs. They appear between $150 \text{ cm}^{-1} < \omega_{\text{RBM}} < 300 \text{ cm}^{-1}$ from the elastically scattered laser line. It corresponds to the vibration of the C atoms in the radial direction, as if the tube is breathing (Figure 3.62). An important point about these modes is the fact that the energy (or wavenumber) of these vibrational modes depends on the diameter (d) of the SWNTs, and not on the way the SWNT is rolled up to form a cylinder, i.e., they do not depend on the θ of the tube.

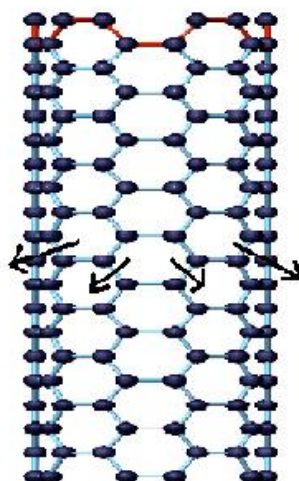


Figure 3.62: Schematic picture showing vibration for RBM. Adapted from A. Jorio, M. A. Pimenta, A. G. S. Filho, R. Saito, G. Dresselhaus, and M. S. Dresselhaus, *New J. Phys.*, 2003, **5**, 139.

These features are very useful for characterizing nanotube diameters through the relation $\omega_{\text{RBM}} = A/d + B$, where A and B are constants and their variations are often attributed to environmental effects, i.e., whether the SWNTs are present as individual tubes wrapped in a surfactant, isolated on a substrate surface, or in the form of bundles. However, for typical SWNT bundles in the diameter range, $d = 1.5 \pm 0.2$ nm, $A = 234 \text{ cm}^{-1} \text{ nm}$ and $B = 10 \text{ cm}^{-1}$ (where B is an upshift coming from tube-tube interactions). For isolated SWNTs on an oxidized Si substrate, $A = 248 \text{ cm}^{-1} \text{ nm}$ and $B = 0$. As can be seen from Figure 3.63, the relation $\omega_{\text{RBM}} = A/d + B$ holds true for the usual diameter range i.e., when d lies between 1 and 2 nm. However, for d less than 1 nm, nanotube lattice distortions lead to chirality dependence of ω_{RBM} and for large diameters tubes when, d is more than 2 nm the intensity of RBM feature is weak and is hardly observable.